PAGEOPH, Vol. 127, Nos. 2/3 (1988)

0033-4553/88/030255-49$1.50 + 0.20/0

A Mathematical Model of the Middle and High Latitude Ionosphere

R. W. SCHUNK [1]

Abstract—A time-dependent three-dimensional model of the middle and high latitude ionosphere is described. The density distributions of six ion species (NO^+, O_2^+, N_2^+, O^+, N^+, He^+) and the electron and ion temperatures are obtained from a numerical solution of the appropriate continuity, momentum and energy equations. The equations are solved as a function of height for an inclined magnetic field at E and F region altitudes. The three-dimensional nature of the model is obtained by following flux tubes of plasma as they convect or corotate through a moving neutral atmosphere. The model takes account of field-aligned diffusion, cross-field electrodynamic drifts, thermospheric winds, polar wind escape, energy-dependent chemical reactions, neutral composition changes, ion production due to solar EUV radiation and auroral precipitation, thermal conduction, diffusion-thermal heat flow and local heating and cooling processes. The model also takes account of the offset between the geomagnetic and geographic poles. A complete description of the ionospheric model is given, including a derivation of the relevant transport equations, formulas for all of the chemical and physical processes contained in the model, a discussion of the numerical technique, and a description of the required model inputs. The effects that various chemical and physical processes have on the ionosphere are also illustrated.

Key words: Ionosphere, thermosphere, model.

1. *Introduction*

The magnetosphere-ionosphere-atmosphere system is strongly coupled via electric fields, particle precipitation, field-aligned currents, heat flows, chemical interactions, and frictional interactions. For example, electric fields of magnetospheric origin induce a large-scale motion of the high-latitude ionosphere, which affects the electron density morphology. As the plasma drifts through the neutrals, the ion temperature is raised owing to ion-neutral frictional heating. The elevated ion temperature then alters the ion chemical reaction rates, which affect the ion composition. Also, particle precipitation in the auroral zone acts to produce enhanced ionization rates and elevated electron temperatures, which affect the electron and ion densities and temperatures. These ionospheric changes, in turn, have a significant effect on the thermospheric structure, circulation, and composition. At F-region altitudes, the neutral atmosphere tends to follow, but lags behind, the convecting ionospheric plasma. The resulting ion-neutral frictional heating induces vertical

[1] Center for Atmospheric and Space Sciences, Utah State University, Logan, Utah 84322-4405 USA.

winds and O/N_2 composition changes. These atmospheric changes then affect the ionospheric density and temperature structure.

The ionosphere-thermosphere system also has a significant effect on the magnetosphere. Precipitating auroral electrons produce conductivity enhancements which can modify the convection electric field, large-scale current systems, and the electrodynamics of the magnetosphere-ionosphere system as a whole. Also, once the thermosphere is set in motion due to convection electric fields, the large inertia of the neutral atmosphere will act to produce dynamo electric fields whenever the magnetosphere tries to change its electrodynamic state. Additional feedback mechanisms occur on polar cap and auroral field lines via a direct flow of plasma from the ionosphere to the magnetosphere. In the polar cap, the continual outflow of thermal plasma from the ionosphere represents a significant source of mass, momentum and energy for the magnetosphere. On auroral field lines, hot ionospheric plasma is injected into the magnetosphere via ion beams, conics, rings, and toroidal distributions.

Although it has been well established that the magnetosphere-ionosphere-atmosphere system is strongly coupled, that time delays occur, and that feedback mechanisms exist, the bulk of the research effort has been directed towards studying the individual elements in the system in a qualitative manner. To date, there have been very few quantitative studies of the coupling between the various regions of the solar-terrestrial system, primarily because of the complexity of the regional models. Nevertheless, considerable progress has been made during the last decade in elucidating the basic physics governing the qualitative behavior of each region. Typically, if one region is studied, the effects of the other regions are parameterized and used as inputs.

At the present time, there are several numerical models of the ionosphere, including auroral models (ROBLE and REES, 1977), *E*-region current-conductivity models (MATSUSHITA and XU, 1982; KAMIDE *et al.*, 1986), high-latitude models (KNUDSEN *et al.*, 1977; WATKINS, 1978; SCHUNK and RAITT, 1980; SOJKA *et al.*, 1981*a*; QUEGAN *et al.*, 1982), mid-latitude models (SCHUNK and WALKER, 1973; ROBLE, 1975; QUEGAN *et al.*, 1982), equatorial models (STERLING *et al.*, 1969; ANDERSON, 1981), and a global model (SOJKA and SCHUNK, 1985).

In this paper, we describe a comprehensive mathematical model of the middle and high latitude ionosphere. This model was initially developed as a mid-latitude, multi-ion (NO^+, O_2^+, N_2^+, and O^+) model by SCHUNK and WALKER (1973). The time-dependent ion continuity and momentum equations were solved as a function of altitude for a corotating plasma flux tube including diurnal variations and many important *E* and *F* region processes. This model was extended to include high latitude effects due to convection electric fields and particle precipitation by SCHUNK *et al.* (1975, 1976). A simplified ion energy equation was also added, which was based on the assumption that local heating and cooling processes dominate (valid below 500 km). Flux tubes of plasma were followed as they moved in response to convection

electric fields. A further extension of the model to include the minor ions N^+ and He^+, an updated photochemical scheme, and the MSIS atmospheric model is described in SCHUNK and RAITT (1980). More recently, the ionospheric model was extended to include the full ion and electron energy equations (SCHUNK and SOJKA, 1982; SCHUNK *et al.*, 1986). The addition of empirical models of plasma convection and particle precipitation is described by SOJKA *et al.* (1981*a*, *b*).

Since the ionospheric model was developed over a fifteen-year period and since the numerical technique was never fully described, it is useful to present the complete updated model in one paper. In Section 2 we present the plasma transport equations upon which the model is based. In Section 3, horizontal plasma convection is discussed, and in Section 4 the ambipolar diffusion equations for vertical plasma transport are derived. Sections 5 and 6 discuss the ion and electron energy equations, respectively. The numerical technique used to solve the equations is given in Section 7, and the required inputs to the model are described in Section 8. Some important model results are given in Section 9. Finally, in Section 10 we give the direction of future model development.

2. *Transport Equations*

The quantitative study of the different flow situations that are found in the terrestrial ionosphere is normally begun through the use of conservation equations which describe the spatial and temporal evolution of the concentration, drift velocity, and temperature of the different species in the ionosphere. These conservation equations are obtained by taking velocity moments of Boltzmann's equation, and the three lowest order equations are the continuity, momentum and energy equations, respectively.

$$\partial n_s/\partial t + \nabla\cdot(n_s\mathbf{u}_s) = P_s' - L_s' n_s \tag{1}$$

$$n_s m_s(D_s\mathbf{u}_s/Dt) + \nabla p_s + \nabla\cdot\vec{\tau}_s - n_s m_s\mathbf{G} - n_s e_s[\mathbf{E} + (1/c)\mathbf{u}_s \times \mathbf{B}] = \delta\mathbf{M}_s/\delta t \tag{2}$$

$$(D_s/Dt)(3p_s/2) + (5/2)p_s(\nabla\cdot\mathbf{u}_s) + \nabla\cdot\mathbf{q}_s + \vec{\tau}_s\!:\nabla\mathbf{u}_s = \delta E_s/\delta t + Q_s - L_s \tag{3}$$

where $D_s/Dt = \partial/\partial t + \mathbf{u}_s\cdot\nabla$ is the convective derivative of species s, $p_s = n_s k T_s$ is the partial pressure, n_s is the number density, m_s is the mass, e_s is the charge, T_s is the temperature, $\mathbf{u}_s$ is the drift velocity, $\mathbf{q}_s$ is the heat flow vector, $\vec{\tau}_s$ is the stress tensor, P_s' is the ionization production rate, L_s' is the ionization loss frequency, Q_s is the heating rate, L_s is the cooling rate; $\mathbf{G}$ is the acceleration due to gravity, $\mathbf{E}$ is the electric field, $\mathbf{B}$ is the magnetic field, $\partial/\partial t$ is the time derivative, ∇ is the coordinate-space gradient, c is the speed of light, and k is Boltzmann's constant. The double-dot operator in equation (3) corresponds to the scalar product of the two tensors (cf.

Table 1

Momentum transfer collision frequencies for electron-neutral interactions

Species	ν_{en}, s^{-1}
N_2	$2.33 \times 10^{-11} n(N_2)[1 - 1.21 \times 10^{-4} T_e] T_e$
O_2	$1.82 \times 10^{-10} n(O_2)[1 + 3.6 \times 10^{-2} T_e^{1/2}] T_e^{1/2}$
O	$8.9 \times 10^{-11} n(O)[1 + 5.7 \times 10^{-4} T_e] T_e^{1/2}$
He	$4.6 \times 10^{-10} n(He) T_e^{1/2}$
H	$4.5 \times 10^{-9} n(H)[1 - 1.35 \times 10^{-4} T_e] T_e^{1/2}$

From SCHUNK and NAGY (1978).

CHAPMAN and COWLING, 1970). The quantities $\delta \mathbf{M}_s/\delta t$ and $\delta E_s/\delta t$ represent the rate of momentum and energy exchange, respectively, in collisions between species s and the other species in the plasma.

In order to calculate collision terms for the transport equations (1)–(3), it is generally necessary to adopt an approximate expression for the species velocity distribution functions. Only for the simplest case of displaced Maxwellians have general collision terms been evaluated that apply to arbitrary interparticle force laws, large temperature differences, and large relative drifts between the interacting species. Fortunately, these collision terms are adequate in the E and F regions of the ionosphere (cf. SCHUNK, 1977, 1983), and the appropriate expressions are given by

$$\delta \mathbf{M}_s/\delta t = \sum_t n_s m_s \nu_{st} (\mathbf{u}_t - \mathbf{u}_s) \Phi_{st} \tag{4}$$

$$\delta E_s/\delta t = n_s m_s \sum_t \nu_{st} [3k(T_t - T_s)\Psi_{st} + m_t (\mathbf{u}_s - \mathbf{u}_t)^2 \Phi_{st}]/(m_s + m_t) \tag{5}$$

where Φ_{st} and Ψ_{st} are velocity-dependent correction factors and ν_{st} is the momentum transfer collision frequency for gases s and t. Expressions for Φ_{st} and Ψ_{st} are given by SCHUNK (1977), but both of these quantities can be set to unity for E and F region studies because of the nature of the collisional processes found in these regions. This is true even in those regions of the high-latitude ionosphere where large convection electric fields exist (cf. SCHUNK, 1983).

In the ionosphere, there are several ion (NO^+, O_2^+, N_2^+, O^+, N^+, He^+, H^+) and neutral (N_2, O_2, O, N, He, H) species, and therefore, the relevant collision processes include Coulomb interactions, nonresonant ion-neutral interactions, resonant charge exchange, and electron-neutral interactions. The appropriate momentum transfer collision frequencies for two-body elastic electron-neutral interactions are given in Table 1. With regard to Coulomb interactions, one needs to consider electron-electron, electron-ion, and ion-ion collisions, and the appropriate expressions are given by (SCHUNK, 1983)

Table 2

The collision frequency coefficients B_{ij} for ion-ion interactions

s^t =	H^+	He^+	N^+	O^+	N_2^+	NO^+	O_2^+
H^+	0.90	1.14	1.23	1.23	1.25	1.25	1.25
He^+	0.28	0.45	0.56	0.57	0.59	0.60	0.60
N^+	0.088	0.16	0.24	0.25	0.28	0.28	0.28
O^+	0.077	0.14	0.22	0.22	0.25	0.26	0.26
N_2^+	0.045	0.085	0.14	0.15	0.17	0.17	0.18
NO^+	0.042	0.080	0.13	0.14	0.16	0.16	0.17
O_2^+	0.039	0.075	0.12	0.13	0.15	0.16	0.16

Table 3

Momentum transfer collision frequencies for resonant ion-neutral interactions

Species	T_r, °K	ν_{in}, s^{-1}
H^+, H	50	$2.65 \times 10^{-10} n(\mathrm{H}) T_r^{1/2}(1 - 0.083 \log_{10} T_r)^2$
He^+, He	50	$8.73 \times 10^{-11} n(\mathrm{He}) T_r^{1/2}(1 - 0.093 \log_{10} T_r)^2$
N^+, N	275	$3.83 \times 10^{-11} n(\mathrm{N}) T_r^{1/2}(1 - 0.063 \log_{10} T_r)^2$
O^+, O	235	$3.67 \times 10^{-11} n(\mathrm{O}) T_r^{1/2}(1 - 0.064 \log_{10} T_r)^2$
N_2^+, N_2	170	$5.14 \times 10^{-11} n(\mathrm{N_2}) T_r^{1/2}(1 - 0.069 \log_{10} T_r)^2$
O_2^+, O_2	800	$2.59 \times 10^{-11} n(\mathrm{O_2}) T_r^{1/2}(1 - 0.073 \log_{10} T_r)^2$
H^+, O	300	$6.61 \times 10^{-11} n(\mathrm{O}) T_i^{1/2}(1 - 0.047 \log_{10} T_i)^2$

$T_r = (T_i + T_n)/2$. From BANKS and KOCHARTS (1973).

$$\nu_{ee} = 54.5 n_e / [\sqrt{2} T_e^{3/2}] \tag{6}$$

$$\nu_{ei} = 54.5 n_i / T_e^{3/2} \tag{7}$$

$$\nu_{ij} = B_{ij} n_j / T_i^{3/2} \tag{8}$$

where subscript e denotes electrons and subscripts i and j correspond to different ion species. The collision frequency coefficients B_{ij} are given in Table 2 for the ion species found in the E and F regions. In equations (6)–(8), the density units are cm^{-3} and temperatures are in °K.

The ion-neutral interactions in the ionosphere can be either resonant or non-resonant, depending on the species involved. Resonant charge exchange occurs when an ion collides with its parent neutral or it can occur accidentally as in the case of the reaction $H^+ + O \rightleftharpoons O^+ + H$. The appropriate resonant ion-neutral momentum transfer collision frequencies are given in Table 3. Non-resonant ion-neutral interactions occur between unlike ions and neutrals, and they correspond to a long-range polarization attraction coupled with a short-range repulsion. In this case, the ion-neutral momentum transfer collision frequencies take a particularly simple form,

Table 4

The collision frequency coefficients $C_{in} \times 10^{10}$ for non-resonant ion-neutral interactions

$i^{n=}$	H	He	N	O	N_2	O_2
H^+	*r*	10.6	26.1	*r*	33.6	32.0
He^+	4.71	*r*	11.9	10.1	16.0	15.3
N^+	1.45	1.49	*r*	4.42	7.47	7.25
O^+	*r*	1.32	4.62	*r*	6.82	6.64
N_2^+	0.74	0.79	2.95	2.58	*r*	4.49
NO^+	0.69	0.74	2.79	2.44	4.34	4.27
O_2^+	0.65	0.70	2.64	2.31	4.13	*r*

r means the collisional interaction is resonant.

$$\nu_{in} = C_{in} n_n \tag{9}$$

where subscript n corresponds to neutrals. The numerical coefficients C_{in} are given in Table 4 for the different ion-neutral combinations found in the ionosphere.

It should be noted that the momentum transfer collision frequencies are not symmetric with respect to a change of indices, but satisfy the relation

$$n_s m_s \nu_{st} = n_t m_t \nu_{ts}. \tag{10}$$

3. *Horizontal Plasma Transport*

At ionospheric altitudes, the earth's dipole magnetic field has an important influence on plasma transport processes (see Figure 1). At mid-latitudes, where the geomagnetic field lines are inclined to the vertical direction, a meridional (north-south) thermospheric wind will act to force the ionization up or down field lines,

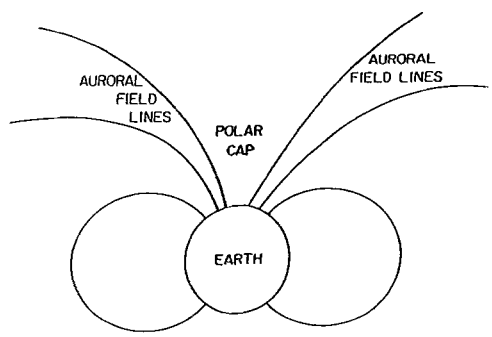

Figure 1
Schematic diagram showing the magnetic field configuration in the near-earth environment.

depending on the direction of the wind. An equatorward wind drives the ionization to higher altitudes where chemical loss rates are lower, while the reverse is true for a poleward wind. The equatorward wind at night therefore acts to maintain the *F*-layer, while the poleward wind during the day acts to depress the *F*-layer. This wind effect competes with field-aligned diffusion and photochemical processes, and the net effect determines the distribution of ionization along a magnetic flux tube. Because magnetospheric electric fields do not play an important role at mid-latitudes, horizontal plasma convection is negligible and the flux tubes of plasma simply corotate with the earth.

At higher latitudes, the plasma does not corotate with the earth, but instead moves in response to magnetospheric electric fields. At ionospheric heights, the magnetospheric (or convection) electric field is directed perpendicular to the geomagnetic field and causes the plasma to drift in the horizontal direction in the manner shown in Figure 2. At all ionospheric altitudes, the electron-neutral collision frequency is much less than the electron cyclotron frequency, and hence, the combined effect of the perpendicular electric field, $\mathbf{E}_\perp$, and geomagnetic field, $\mathbf{B}$, is to induce an electron drift in the $\mathbf{E}_\perp \times \mathbf{B}$ direction. For the ions, on the other hand, the different ion-neutral collision frequencies are greater than corresponding cyclotron frequencies at low altitudes (*E* region), with the result that the ions drift in the direction of the perpendicular electric field. As altitude increases, the ion velocity

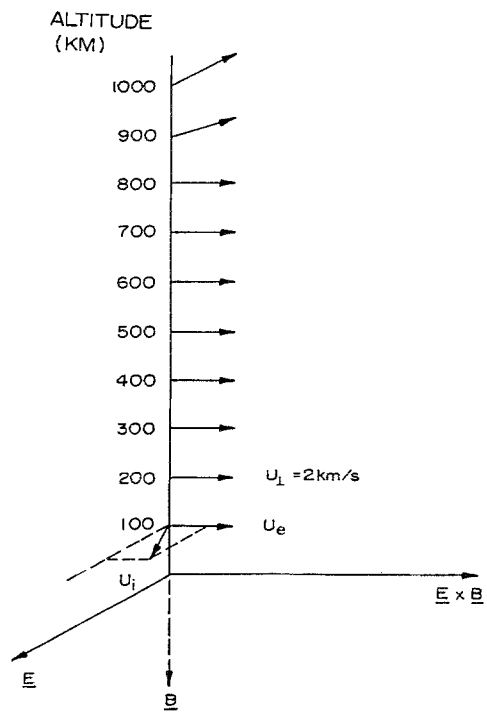

Figure 2
Ion and electron drift velocities as a function of altitude in the high latitude ionosphere.

vectors rotate toward the $\mathbf{E}_\perp \times \mathbf{B}$ direction owing to the decreasing ion-neutral collision frequencies. At F region altitudes ($\gtrsim$160 km), both ions and electrons drift in the $\mathbf{E}_\perp \times \mathbf{B}$ direction. At still greater heights ($\gtrsim$800 km), the plasma begins to flow out of the topside ionosphere with a speed that increases with altitude (the polar wind).

The electromagnetic drift described above must, in general, compete with both horizontal diffusion and the diamagnetic drift driven by perpendicular pressure gradients. In order to compare the transport processes, it is convenient to make the following simplifying assumptions: (a) The neutral atmosphere is stationary ($\mathbf{u}_n = 0$); (b) Steady state conditions prevail ($\partial \mathbf{u}_i/\partial t = 0$); (c) The flow is subsonic ($\mathbf{u}_i \cdot \nabla \mathbf{u}_i \rightarrow 0$); (d) The ionosphere is isothermal; and (e) Stress effects are negligible ($\vec{\tau}_i = 0$).

With the above simplifying assumptions, the momentum equation (2) for the horizontal motion of a given ion species (subscript i) reduces to

$$kT_i \nabla_\perp n_i - e_i n_i [\mathbf{E}_\perp + (1/c)\mathbf{u}_i \times \mathbf{B}] = -n_i m_i \nu_{in} \mathbf{u}_i. \tag{11}$$

This equation can also be expressed in the following form:

$$\mathbf{u}_i = -(D_i/n_i)\nabla_\perp n_i + \mu_i \mathbf{E}_\perp + (\Omega_i/\nu_{in})(\mathbf{u}_i \times \mathbf{b}) \tag{12}$$

where the ion diffusion coefficient, D_i, mobility coefficient, μ_i, and cyclotron frequency, Ω_i, are given by

$$D_i = kT_i/(m_i \nu_{in}) \tag{13}$$

$$\mu_i = e_i/(m_i \nu_{in}) \tag{14}$$

$$\Omega_i = e_i B/(m_i c). \tag{15}$$

Equation (12) can be readily solved by expressing this equation in terms of the individual velocity components. The solution to this equation is given by

$$\mathbf{u}_i = -(D_{i\perp}/n_i)\nabla_\perp n_i + \mu_{i\perp}\mathbf{E}_\perp + (\mathbf{u}_E + \mathbf{u}_{iD})/(1 + \nu_{in}^2/\Omega_i^2) \tag{16}$$

where the electromagnetic drift, $\mathbf{u}_E$, and diamagnetic drift, $\mathbf{u}_{iD}$, are given by

$$\mathbf{u}_E = c(\mathbf{E} \times \mathbf{B})/B^2 \tag{17}$$

$$\mathbf{u}_{iD} = -c(\nabla_\perp p_i \times \mathbf{B})/(e_i n_i B^2) \tag{18}$$

and where

$$D_{i\perp} = D_i/(1 + \Omega_i^2/\nu_{in}^2) \tag{19}$$

$$\mu_{i\perp} = \mu_i/(1 + \Omega_i^2/\nu_{in}^2). \tag{20}$$

An equation similar to (16) holds for the electrons.

At altitudes above about 160 km, $\nu_{in}/\Omega_i \ll 1$. Also, a comparison of the terms in equation (16) for altitudes above 160 km indicates that the electromagnetic drift is the dominant term for both ions and electrons if the scale length for horizontal

variations is greater than a few km. In our ionospheric model, we assume that the horizontal motion of the ionosphere is determined solely by the electromagnetic drift (17), and therefore, our model is rigorous only above 160 km and is limited to large-scale horizontal structures (>10 km). In practice, however, the model can be applied to altitudes as low as 120 km in sunlit regions and in the auroral oval owing to the dominance of chemical processes over transport processes at low altitudes. Only in the dark polar regions, where there is little ion production, is the model not rigorously valid below 160 km. At mid-latitudes, however, the model is valid throughout the E and F regions because horizontal transport is negligible.

An important feature of the plasma motion associated with the electromagnetic drift is that the flow is essentially incompressible (RISHBETH and HANSON, 1974). This feature allows one to follow individual flux tubes of plasma as they convect horizontally across the polar regions. A time-dependent three-dimensional picture of the polar ionosphere can be constructed simply by following many plasma flux tubes.

The incompressible nature of the electromagnetic drift can be shown by taking the divergence of equation (17),

$$\nabla \cdot \mathbf{u}_E = \nabla \cdot [c(\mathbf{E} \times \mathbf{B})/B^2] \tag{21}$$

$$= \frac{c}{B^2} [\mathbf{B} \cdot (\nabla \times \mathbf{E}) - \mathbf{E} \cdot (\nabla \times \mathbf{B})] + c(\mathbf{E} \times \mathbf{B}) \cdot \nabla \left(\frac{1}{B^2} \right). \tag{22}$$

For an electrostatic field, $\nabla \times \mathbf{E} = 0$. Also, $\nabla \times \mathbf{B} \sim \mathbf{J}$, $\mathbf{J} \parallel \mathbf{B}$ at F-region altitudes in the auroral oval, and $\mathbf{E} \perp \mathbf{B}$, and therefore, $\mathbf{E} \cdot (\nabla \times \mathbf{B}) = 0$. The last term in equation (22) represents compression (rarefaction) as the plasma drifts into a region of greater (smaller) B, and RISHBETH and HANSON (1974) have shown that this term is small in the F-region. Therefore, at ionospheric altitudes,

$$\nabla \cdot \mathbf{u}_E \approx 0, \tag{23}$$

and the electrodynamic drift is incompressible.

4. Plasma Diffusion Equations

As noted earlier, above about 160 km the ion and electron collision frequencies are much smaller than the corresponding cyclotron frequencies, and consequently, the plasma is constrained to move along geomagnetic field lines like beads on a string, except when electric fields cause the entire ionosphere to convect horizontally. However, this latter motion is distinct from the field-aligned motion and the two can simply be added vectorally. The field-aligned motion is influenced by gravity as well as vertical density and temperature gradients. Owing to the small electron mass, the effect of gravity is to cause a charge separation, with the lighter electrons tending to settle on top of the heavier ions. However, a polarization electrostatic field develops

which acts to prevent a large charge separation. Once this electrostatic field has developed, the ions and electrons move together as a single gas under the influence of gravity and the density and temperature gradients. Such a motion is called ambipolar diffusion.

In the ionosphere, which is a partially-ionized plasma, it is convenient to distinguish between major and minor ions. A major ion is a species whose density is comparable to the electron density, and consequently, it is important in maintaining charge neutrality in the plasma. A minor ion, on the other hand, is essentially a trace species whose density is much smaller than that of the electrons, and hence, its contribution to charge neutrality is negligibly small. In what follows, we will derive separate diffusion equations for the major and minor ions.

4.1. Major Ion Diffusion

When following convecting or corotating plasma flux tubes, it is convenient to express the ion continuity equation (1) in the following form:

$$\frac{\partial n_i}{\partial t} + \mathbf{u}_{i\perp} \cdot \nabla_\perp n_i + n_i(\nabla \cdot \mathbf{u}_{i\perp}) + \nabla_\parallel \cdot (n_i \mathbf{u}_{i\parallel}) = P_i' - L_i' n_i \tag{24}$$

where the subscripts $\parallel$ and $\perp$ refer to the directions parallel and perpendicular to **B**, respectively. At middle and high latitudes, the perpendicular ion motion results from either convection or corotation electric fields, and for such fields $\nabla \cdot \mathbf{u}_{i\perp} = 0$ [equation (23)]. Therefore, equation (24) reduces to

$$\frac{D_i n_i}{Dt} + \nabla_\parallel \cdot (n_i \mathbf{u}_{i\parallel}) = P_i' - L_i' n_i \tag{25}$$

where $D_i/Dt = (\partial/\partial t + \mathbf{u}_{i\perp} \cdot \nabla)$ is the convective derivative for horizontal motion; that is, the appropriate derivative for following convecting plasma flux tubes.

With regard to the momentum equation (2) for field-aligned plasma motion, several simplifications are possible. First, when studying large-scale ionospheric behavior, one is generally not interested in plasma wave phenomena, so the $\partial \mathbf{u}_i/\partial t$ term in the momentum equation can be neglected. Also, the ion motion along **B** is subsonic at E and F region altitudes. The simplification associated with subsonic flow can be seen by comparing the nonlinear inertial term with the pressure-gradient term in equation (2). Assuming that $\nabla_\parallel \sim 1/L$, where L is a characteristic length, the ratio of these two terms is

$$n_i m_i (\mathbf{u}_{i\parallel} \cdot \nabla_\parallel) u_{i\parallel} / \nabla_\parallel p_i \sim u_{i\parallel}^2 / (kT_i/m_i) = M_i^2 \tag{26}$$

where M_i is the Mach number of the ion flow. Therefore, if the ion flow is subsonic, the nonlinear inertial term can be neglected. With the above simplifications, the ion

momentum equation reduces to

$$\nabla_{\|} p_i + (\nabla \cdot \vec{\tau}_i)_{\|} - n_i m_i \mathbf{G}_{\|} - n_i e_i \mathbf{E}_{\|} = n_i m_i \sum_n \nu_{in} (\mathbf{u}_n - \mathbf{u}_i)_{\|} \tag{27}$$

where Coulomb collisions between the major ion species have been omitted in equation (27). As shown by SCHUNK and WALKER (1973), ion-neutral collisions dominate the momentum transfer in the E and F regions.

In order to obtain a self-consistent set of ion diffusion equations, it is necessary to have an expression for the polarization electrostatic field $\mathbf{E}_{\|}$. Since the electron mobility along $\mathbf{B}$ is much greater than the ion mobility, this electrostatic field is determined by the electrons. Substituting $s = e$ in equation (2) and neglecting terms containing the small electron mass, the equation for $\mathbf{E}_{\|}$ reduces to

$$e\mathbf{E}_{\|} = -\frac{1}{n_e} \nabla_{\|} p_e \tag{28}$$

where $p_e = n_e k T_e$ is the electron pressure and $n_e = \Sigma_i n_i$, with the sum being over the major ion species.

Substituting equation (28) into (27), setting $p_i = n_i k T_i$ and $p_e = n_e k T_e$, and solving for the ion drift velocity, we obtain

$$\mathbf{u}_{i\|} = \mathbf{u}_{n\|} - D_i \left[\frac{1}{n_i} \nabla_{\|} n_i + \frac{(\nabla \cdot \vec{\tau}_i)_{\|}}{n_i k T_i} - \frac{m_i \mathbf{G}_{\|}}{k T_i} + \frac{1}{T_i} \nabla_{\|} (T_e + T_i) + \frac{(T_e/T_i)}{n_e} \nabla_{\|} n_e \right] \tag{29}$$

where

$$D_i = k T_i / (m_i \sum_n \nu_{in}) \tag{30}$$

is a generalization of the ion diffusion coefficient given in equation (13). In deriving equation (29), we assumed that the different neutral species in the earth's ionosphere have a common drift velocity, which is a reasonable assumption.

The ion tensor $\vec{\tau}_i$ accounts for electric field induced stress, which arises from ion-neutral collisions. If vertical gradients in the plasma are more important than horizontal gradients, then only the tensor element associated with the $\mathbf{B}$ direction enters in equation (29), i.e., only the $\vec{\tau}_i$: **BB** element. This parallel component has been calculated by SCHUNK (1975) for the case where the various neutral species have displaced Maxwellian velocity distributions with a common temperature and a common drift velocity,

$$\tau_{i\parallel} = \frac{R_i}{S_i + 0.6\nu_{ii}} n_i m_i \left[(u_i - u_n)_\parallel^2 - \frac{1}{3}(\mathbf{u}_i - \mathbf{u}_n)^2 \right] \tag{31}$$

where

$$R_i = \sum_n \frac{m_n \nu_{in}}{m_i + m_n} \left[1 - \frac{3}{4} \frac{Q_{in}^{(2)}}{Q_{in}^{(1)}} \right] \tag{32}$$

$$S_i = \sum_n \frac{m_i \nu_{in}}{m_i + m_n} \left[1 + \frac{3}{4} \frac{m_n}{m_i} \frac{Q_{in}^{(2)}}{Q_{in}^{(1)}} \right] \tag{33}$$

and where ν_{ii} is the ion self-collision frequency (equation 8) and $Q_{in}^{(2)}/Q_{in}^{(1)}$ is the ratio of collision cross-sections (cf. SCHUNK, 1975). Coulomb interactions are important only at high altitudes and only for electric fields less than about 50 mVm^{-1}. Therefore, the ν_{ii} term in equation (31) needs to be included in the O^+ stress tensor, but not in the molecular ion stress tensors. For a mixture of NO^+ or O_2^+ with either N_2 or O_2, $R_i/S_i \approx \frac{1}{4}$.

For most ionospheric applications, the contribution of $(u_i - u_n)_\parallel^2$ to the parallel component of the ion stress tensor (31) can be neglected because this term is usually small. The main contribution arises from the relative ion-neutral drift induced by perpendicular electric fields. In this case, equation (31) can be expressed in the following form (SCHUNK *et al.*, 1975):

$$\tau_{i\parallel} = -\frac{1}{3} \frac{R_i n_i m_i}{S_i + 0.6\nu_{ii}} \frac{(E'_\perp c/B)^2}{1 + \nu_i^2/\Omega_i^2} \tag{34}$$

where $\nu_i = \Sigma_n \nu_{in}$ and $\mathbf{E}'_\perp$ is an effective electric field,

$$\mathbf{E}'_\perp = \mathbf{E}_\perp + (1/c)\mathbf{u}_n \times \mathbf{B}. \tag{35}$$

In summary, the continuity and momentum equations for the various major ion species are obtained by separately applying equations (25), (29), (30) and (34) to these species. Since $n_e = \Sigma_i n_i$, the major ion transport equations are coupled and nonlinear.

4.2. Minor Ion Diffusion

The continuity equation for a minor ion is identical to the major ion continuity equation (25) and need not be repeated. The minor ion diffusion equation is similar to that of the major ions, but there are some important differences. Since its derivation is similar to that described above, we will merely give the final result. Also, for convenience, we will consider a specific minor ion, N^+, so that specific expressions can be given.

For N^+, the momentum equation for motion along **B** is given by SCHUNK and

RAITT (1980),

$$\mathbf{u}_{\parallel}(\mathrm{N}^+) = \sum_t v(\mathrm{N}^+, t)\mathbf{u}_{t\parallel}/v(\mathrm{N}^+) - D(\mathrm{N}^+)\left[\frac{1}{n(\mathrm{N}^+)}\nabla_{\parallel} n(\mathrm{N}^+) + \frac{(\nabla\cdot\vec{\tau}(\mathrm{N}^+))_{\parallel}}{n(\mathrm{N}^+)kT_i} - \frac{m(\mathrm{N}^+)\mathbf{G}_{\parallel}}{kT_i} + \frac{1}{T_i}\nabla_{\parallel}(T_e + T_i) + \frac{(T_e/T_i)}{n_e}\nabla_{\parallel} n_e\right] \tag{36}$$

where

$$D(\mathrm{N}^+) = kT_i/m(\mathrm{N}^+)v(\mathrm{N}^+) \tag{37}$$

$$v(\mathrm{N}^+) = \sum_t v(\mathrm{N}^+, t) \tag{38}$$

and where the various ion species were assumed to have a common temperature. Also, in equations (36) and (38), the summation is over both the major ion and neutral species. One important difference between the minor ion (36) and major ion (29) diffusion equations is that the major ions tend to drag the minor ions with them when they diffuse along **B** (first term in equation 36). Another difference is that as the minor ions try to diffuse in response to density and temperature gradients, their motion is impeded not only by the neutrals, but also by the major ions (equations 37 and 38). Perhaps the most significant difference is that the polarization electrostatic field ($\nabla_{\parallel} n_e$ term) is determined by the major ions and is an input to the minor ion equation (36). Therefore, the minor ion diffusion equation does not have the strong nonlinearity that the major ion equation has. Consequently, minor ion diffusion equations are easily solved numerically.

The major ions also affect the expression for the minor ion stress tensor. For a minor ion N^+ in an O^+ dominated plasma, the parallel stress tensor component is given by SCHUNK and RAITT (1980)

$$\tau_{\parallel}(\mathrm{N}^+) = -\frac{(1/3)R(\mathrm{N}^+)n(\mathrm{N}^+)m(\mathrm{N}^+)u_{\perp}^2 - 0.2n(\mathrm{N}^+)v(\mathrm{N}^+, \mathrm{O}^+)\tau_{\parallel}(\mathrm{O}^+)/n(\mathrm{O}^+)}{S(\mathrm{N}^+) + 0.6v(\mathrm{N}^+, \mathrm{N}^+) + 0.8v(\mathrm{N}^+, \mathrm{O}^+)} \tag{39}$$

where

$$R(\mathrm{N}^+) = 0.27v(\mathrm{N}^+, \mathrm{N}_2) + 0.28v(\mathrm{N}^+, \mathrm{O}_2) + 0.21v(\mathrm{N}^+, \mathrm{O}) \tag{40}$$

$$S(\mathrm{N}^+) = 0.73v(\mathrm{N}^+, \mathrm{N}_2) + 0.72v(\mathrm{N}^+, \mathrm{O}_2) + 0.79v(\mathrm{N}^+, \mathrm{O}) \tag{41}$$

$$u_{\perp}^2 = \frac{(E'_{\perp}c/B)^2}{1 + v'^2/\Omega^2} \tag{42}$$

$$v' = v(\mathrm{N}^+, \mathrm{N}_2) + v(\mathrm{N}^+, \mathrm{O}_2) + v(\mathrm{N}^+, \mathrm{O}) \tag{43}$$

$$\Omega = eB/m(\mathrm{N}^+)c. \tag{44}$$

4.3. Vertical Plasma Gradients and Inclined **B**

At middle and high latitudes, plasma gradients in the vertical direction tend to be much more important than horizontal gradients. The vertical gradients, in combination with an inclined magnetic field, affect the ion motion in several ways. First, the effectiveness of diffusion is reduced because the density and temperature gradients are in the vertical direction, while the ions can move only along the inclined geomagnetic field lines. The inclination of **B** is described by the magnetic field dip angle I, which is defined relative to the horizontal direction ($I = 0°$ at the magnetic equator and 90° at the poles). If the gradients in the plasma are in the vertical (z) direction, then the ion continuity (25) and momentum (29) equations are applicable provided the ion diffusion coefficients are multiplied by $\sin^2 I$ (cf. RISHBETH and GARRIOTT, 1969).

Another consequence of an inclined **B** is that meridional (or north-south) neutral winds can induce a vertical plasma drift. If V is the southward component of the neutral wind, the induced plasma drift along **B** is $V \cos I$ and the associated vertical plasma drift is $V \cos I \sin I$. During the day the wind blows from the equator to the poles, which induces a downward plasma drift, while the reverse occurs at night.

A third consequence of an inclined **B** relates to convection electric fields. Since the plasma **E** × **B** drift is perpendicular to **B**, an inclined **B** produces a vertical **E** × **B** drift component. If E_y is an eastward electric field component, then the vertical ion drift induced by this component is $(cE_y/B) \cos I$, which is positive in the upward direction.

In summary, in a cartesian coordinate system with x southward, y eastward, and z upward, the ion momentum equation (29) for vertical plasma gradients, a southward wind component, and an eastward electric field component becomes

$$u_{iz} = \frac{cE_y}{B} \cos I + V \cos I \sin I - D_i \sin^2 I \left[\frac{1}{n_i} \frac{\partial n_i}{\partial z} + \frac{\partial \tau_{i\|}/\partial z}{n_i k T_i} + \frac{m_i g}{k T_i} + \frac{1}{T_i} \frac{\partial}{dz} (T_e + T_i) + \frac{(T_e/T_i)}{n_e} \frac{\partial n_e}{\partial z} \right] \tag{45}$$

where g is the magnitude of the gravitational acceleration, which is downward. Equation (45) is the basic momentum equation in our ionospheric model for the major ions, and a similar modification of equation (36) is used for the minor ions.

In general, the earth's magnetic field has both an inclination and a declination. The latter, in combination with electric fields and neutral winds, also acts to produce vertical plasma drifts (cf. RISHBETH and GARRIOTT, 1969), but these are usually smaller than those given in equation (45). Nevertheless, these additional plasma drifts have been included in our ionospheric model even though they are typically small.

4.4. *Photochemistry*

Solar extreme ultraviolet (EUV) radiation photoionizes the neutral constituents of the upper atmosphere, producing free electrons and ions. The photoionization process occurs predominantly at the lower levels of the ionosphere, where the neutrals are abundant. Typically, the peak in the ionization rate occurs at about 150 km owing mainly to the absorption of radiation with wavelengths less than 796 Å (the ionization threshold of N_2). Photons with wavelengths in the range of 796–1027 Å penetrate down into the E region. For the E and F regions of the ionosphere, the most important photoionization processes are

$$N_2 + h\nu \rightarrow N_2^+ + e \tag{46a}$$

$$\rightarrow N^+ + N + e \tag{46b}$$

$$O_2 + h\nu \rightarrow O_2^+ + e \tag{47}$$

$$O + h\nu \rightarrow O^+ + e \tag{48}$$

$$N + h\nu \rightarrow N^+ + e \tag{49}$$

where (46b) is produced with an efficiency of about 21% (McElroy, 1967).

The calculation of the photoionization rates requires a knowledge of the number densities of the neutral constituents, n_n, as a function of altitude z, the absorption $\sigma_n^{(a)}(\lambda)$ and ionization $\sigma_n^{(i)}(\lambda)$ cross-sections of these constituents as a function of wavelength λ, and the spectrum of solar radiation incident on the top of the atmosphere $I_\infty(\lambda)$. In terms of these quantities, the ion production rate is given by

$$q_i'(z) = n_n(z) \int_0^\infty d\lambda I_\infty(\lambda) \sigma_n^{(i)}(\lambda) \exp[-\tau(\lambda, z)] \tag{50}$$

where the optical depth τ is given by

$$\tau(\lambda, z) = \sum_n \sigma_n^{(a)}(\lambda) n_n(z) H_n \mathrm{ch}(R_n, \chi) \tag{51}$$

and where

$$H_n = kT_n/m_n g \tag{52}$$

$$R_n = (R_e + z)/H_n. \tag{53}$$

In (50)–(53), R_e is the radius of the earth, χ is the solar zenith angle, and $\mathrm{ch}(R_n, \chi)$ is the Chapman grazing incidence function (Chapman, 1931). Approximate expressions for the Chapman function, valid for both large and small solar zenith angles, have been presented by F. L. Smith and C. Smith (1972). For $\chi < 80°$ the Chapman

Table 5

Weighted photoionization and photoabsorption cross-sections ($\sigma_{eff}/10^{-18}$ cm^2)

	Species:	O^+ (4S)	O^+ (2D)	O^+ (2P)	Tot. O^+	He^+	N_2 (ABS)	N_2 (ION)	O_2 (ABS)	O_2 (ION)
Interval	$\Delta\lambda$, A									
1	50–100	0.32	0.34	0.22	1.06	0.21	0.60	0.60	1.18	1.18
2	100–150	1.03	1.14	0.75	3.53	0.53	2.32	2.32	3.61	3.61
3	150–200	1.62	2.00	1.30	5.96	1.02	5.40	5.40	7.27	7.27
4	200–250	1.95	2.62	1.70	7.55	1.71	8.15	8.15	10.50	10.50
5	256.3	2.15	3.02	1.95	8.43	2.16	9.65	9.65	12.80	12.80
6	284.15	2.33	3.39	2.17	9.26	2.67	10.60	10.60	14.80	14.80
7	250–300	2.23	3.18	2.04	8.78	2.38	10.08	10.08	13.65	13.65
8	303.31	2.45	3.62	2.32	9.70	3.05	11.58	11.58	15.98	15.98
9	303.78	2.45	3.63	2.32	9.72	3.05	11.60	11.60	16.00	16.00
10	300–350	2.61	3.98	2.52	10.03	3.65	14.60	14.60	17.19	17.19
11	368.07	2.81	4.37	2.74	10.84	4.35	18.00	18.00	18.40	18.40
12	350–400	2.77	4.31	2.70	10.70	4.25	17.51	17.51	18.17	18.17
13	400–450	2.99	4.75	2.93	11.21	5.51	21.07	21.07	19.39	19.39
14	465.22	3.15	5.04	3.06	11.25	6.53	21.80	21.80	20.40	20.40
15	450–500	3.28	5.23	3.13	11.64	7.09	21.85	21.85	21.59	21.59
16	500–550	3.39	5.36	3.15	11.91	0.72	24.53	24.53	24.06	24.06
17	554.37	3.50	5.47	3.16	12.13	0.00	24.69	24.69	25.59	25.59
18	584.33	3.58	5.49	3.10	12.17	0.00	23.20	23.20	22.00	22.00
19	550–600	3.46	5.30	3.02	11.90	0.00	22.38	22.38	25.04	25.04
20	609.76	3.67	5.51	3.05	12.23	0.00	23.10	23.10	26.10	26.10
21	629.73	3.74	5.50	2.98	12.22	0.00	23.20	23.20	25.80	25.80
22	600–650	3.73	5.50	2.97	12.21	0.00	23.22	23.22	26.02	25.94
23	650–700	4.04	5.52	0.47	10.04	0.00	29.75	25.06	26.27	22.05
24	703.36	4.91	6.44	0.00	11.35	0.00	26.30	23.00	25.00	23.00
25	700–750	4.20	3.80	0.00	8.00	0.00	30.94	23.20	29.05	23.81
26	765.15	4.18	0.00	0.00	4.18	0.00	35.46	23.77	21.98	8.59
27	770.41	4.18	0.00	0.00	4.18	0.00	26.88	18.39	25.18	9.69
28	789.36	4.28	0.00	0.00	4.28	0.00	19.26	10.18	26.66	11.05
29	750–800	4.23	0.00	0.00	4.23	0.00	30.71	16.75	27.09	9.39
30	800–850	4.38	0.00	0.00	4.38	0.00	15.05	0.00	20.87	6.12
31	850–900	4.18	0.00	0.00	4.18	0.00	46.63	0.00	9.85	4.69
32	900–950	2.12	0.00	0.00	2.12	0.00	16.99	0.00	15.54	9.34
33	977.62	0.00	0.00	0.00	0.00	0.00	0.70	0.00	4.00	2.50
34	950–1000	0.00	0.00	0.00	0.00	0.00	36.16	0.00	16.53	12.22
35	1025.72	0.00	0.00	0.00	0.00	0.00	0.00	0.00	1.60	1.00
36	1031.91	0.00	0.00	0.00	0.00	0.00	0.00	0.00	1.00	0.00
37	1000–1050	0.00	0.00	0.00	0.00	0.00	0.00	0.00	1.10	0.27

From TORR *et al.* (1979*a*).

Table 6

Ion Chemistry and Reaction Rates. From SCHUNK and RAITT [1980].

	Reaction	Rate Coefficients, $cm^3\ s^{-1}$	Source
0	$O^+ + N_2 \rightarrow NO^+ + O$	k_1 O+ + N2 -> NO+ N	(a)
1	$O^+ + O_2 \rightarrow O_2^+ + O$	k_2	(a)
2	$O^+ + NO \rightarrow NO^+ + O$	k_3	(a)
3	$O_2^+ + N_2 \rightarrow NO^+ + NO$	5×10^{-16}	(b)
4	$O_2^+ + NO \rightarrow NO^+ + O_2$	4.4×10^{-10}	(c)
5	$O_2^+ + N \rightarrow NO^+ + O$	1.2×10^{-10}	(d)
6	$O_2^+ + e \rightarrow O + O$	$1.6 \times 10^{-7}\ (300/T_e)^{0.55}$	(e)
7	$N_2^+ + O \rightarrow NO^+ + N$	$1.4 \times 10^{-10}\ (300/T)^{0.44}$; $T \leq 1500°$ K	
		$5.2 \times 10^{-11}\ (T/300)^{0.2}$; $T > 1500°$ K	(f)
8	$N_2^+ + O \rightarrow O^+ + N_2$	$1 \times 10^{-11}\ (300/T)^{0.23}$; $T \leq 1500°$ K	
		$3.6 \times 10^{-12}\ (T/300)^{0.41}$; $T > 1500°$ K	(f)
9	$N_2^+ + O_2 \rightarrow O_2^+ + N_2$	$5 \times 10^{-11}\ (300/T)$	(g)
10	$N_2^+ + NO \rightarrow NO^+ + N_2$	3.3×10^{-10}	(h)
11	$N_2^+ + e \rightarrow N + N$	$1.8 \times 10^{-7}\ (300/T_e)^{0.39}$	(i)
12	$NO^+ + e \rightarrow N + O$	$4.2 \times 10^{-7}\ (300/T_e)^{0.85}$	(j)
13	$He^+ + N_2 \rightarrow N^+ + N + He$	1×10^{-9}	(c)
14	$N^+ + O_2 \rightarrow NO^+ + O$	2×10^{-10}	(c)
15	$N^+ + O_2 \rightarrow O_2^+ + N$	4×10^{-10}	(c)
16	$N^+ + NO \rightarrow NO^+ + N$	2×10^{-11}	(k)

(a) ALBRITTON *et al.* [1977]; ST.-MAURICE and TORR [1978].
(b) FITE [1969].
(c) LINDINGER *et al.* [1974]; HUNTRESS and ANICICH [1976].
(d) FEHSENFELD [1977].
(e) MEHR and BIONDI [1969]: WALLS and DUNN [1974]; TORR *et al.* [1976b].
(f) MCFARLAND *et al.* [1974]; TORR *et al.* [1977].
(g) MCFARLAND *et al.* [1973]; LINDINGER *et al.* [1974].
(h) FEHSENFELD *et al.* [1970].
(i) MEHR and BIONDI [1969].
(j) WALLS and DUNN [1974]; TORR *et al.* [1976a].
(k) KOSMIDER and HASTED [1975].

function can be replaced by $\sec \chi$ in every term in the summation in (51).

For numerical computations of q_i', the solar spectrum was divided into the 37 wavelength intervals suggested by TORR *et al.* (1979*a*). The photon fluxes in these intervals were obtained from the Atmosphere Explorer satellite measurements of HINTEREGGER *et al.* (1977) and HEROUX and HINTEREGGER (1978) for low solar activity. These fluxes were scaled for higher levels of solar activity. The photoionization and photoabsorption cross-sections we adopted were obtained from KIRBY-DOCKEN *et al.* (1978) and these values are given in Table 5 for the main neutral constituents. For atomic nitrogen we adopted the photoionization cross-sections calculated by HENRY (1968), which are in good agreement with the experimental results of COMES and ELZER (1968).

We have also included a 'nocturnal' ionization source due to resonantly scattered

solar radiation, but for this source we merely adopted the ionization rates presented by CHEN and HARRIS (1971) and assumed they do not vary throughout the night. The production rate of NO^+ has a peak value of 0.6 cm^{-3} s^{-1} at 98 km. The O_2^+ peak production rate is 1.8 cm^{-3} s^{-1}, which occurs at 108 km.

After ions are created by either photoionization or impact ionization due to precipitating energetic particles, there are numerous chemical reactions that occur and they act to create new ions and destroy old ones. The chemical reactions included in our ionospheric model are given in Table 6 along with the reaction rates and associated references. The rates for O^+ reactions with N_2, O_2 and NO have a complicated temperature dependence and these are given by

$$k_1 = 1.533 \times 10^{-12} - 5.92 \times 10^{-13}(T/300) + 8.60 \times 10^{14}(T/300)^2; \quad 300 \leqslant T \leqslant 1700°K \tag{54a}$$

$$k_1 = 2.73 \times 10^{-12} - 1.155 \times 10^{-12}(T/300) + 1.483 \times 10^{-13}(T/300)^2; \quad 1700 < T < 6000°K \tag{54b}$$

$$k_2 = 2.82 \times 10^{-11} - 7.74 \times 10^{-12}(T/300) + 1.073 \times 10^{-12}(T/300)^2 - 5.17 \times 10^{-14}(T/300)^3 + 9.65 \times 10^{-16}(T/300)^4; \quad 300 \leqslant T \leqslant 6000°K \tag{55}$$

$$k_3 = 8.36 \times 10^{-13} - 2.02 \times 10^{-13}(T/300) + 6.95 \times 10^{-14}(T/300)^2; \quad 320 < T < 1500°K \tag{56a}$$

$$k_3 = 5.33 \times 10^{-13} - 1.64 \times 10^{-14}(T/300) + 4.72 \times 10^{-14}(T/300)^2 - 7.05 \times 10^{-16}(T/300)^3; \quad 1500 < T < 6000°K \tag{56b}$$

where T is the effective temperature (cf. SCHUNK *et al.*, 1975). In equations (54)–(56), the effective temperature is given by

$$T = T(O^+) + \frac{m(O^+)}{m(O^+) + m_r} \frac{m_r - m_b}{3k} u_\perp^2(O^+), \tag{57}$$

where

$$m_b = \frac{\Sigma_n \dfrac{m_n \nu(O^+, n)}{m(O^+) + m_n}}{\Sigma_n \dfrac{\nu(O^+, n)}{m(O^+) + m_n}} \tag{58}$$

and where m_r is the reactant mass (N_2, O_2, or NO mass) and $T(O^+)$ is the O^+ temperature. It should be noted that the effective temperature is different for the three reactions in equations (54) to (56) because of the presence of m_r.

The expression for the effective temperature takes a particularly simple form at altitudes above about 200 km, where $\nu_i/\Omega_i \ll 1$ and where atomic oxygen is the dominant neutral species impeding the flow of O^+ [$m_b \rightarrow m(O)$]. Setting $m_r = m(N_2)$,

$B = 0.5$ gauss and assuming the O^+ perpendicular drift is due to $\mathbf{E} \times \mathbf{B}$ motion, the expression for T becomes

$$T = T_n + 0.329E_\perp'^2 \quad (v_i/\Omega_i \ll 1) \tag{59}$$

with $E_\perp'$ in mVm^{-1}. For large electric field strengths, $T \sim E_\perp'^2$ and $k_1 \sim E_\perp'^4$.

When atomic oxygen is photoionized, about half of the O^+ ions produced are in the ^4S state, while the other half are in the ^2D state (BANKS and KOCKARTS, 1973). In our early model studies, $O^+(^2D)$ was assumed to react rapidly with N_2 (RUTHERFORD and VROOM, 1971), and consequently, these ions provided an enhanced N_2^+ production rate. However, studies of the mid-latitude ionosphere using Atmosphere Explorer data suggest that the $O^+(^2D) + N_2$ reaction may be much slower than previously thought (TORR and ORSINI, 1978). Although this result has not been confirmed for all conditions encountered by the AE satellites, the consequence of a lower $O^+(^2D) + N_2$ reaction rate is that electron quenching of $O^+(^2D)$ becomes important at low altitudes, which means the fraction of $O^+(^2D)$ converted into N_2^+ depends on the ambient electron density.

At mid-latitudes the seasonal variation of N_mF_2 results in about 25% of $O^+(^2D)$ being converted into N_2^+ in winter and about 75% in summer (D. G. Torr, private communication). We adopted these conversion values so that our model would yield the expected seasonal behavior when applied to mid-latitudes. However, at high-latitudes the electron density exhibits significant variation with ionospheric and atmospheric conditions, and consequently, the fraction of $O^+(^2D)$ converted into N_2^+ is also expected to vary with these conditions. Therefore, we did several model calculations varying the $O^+(^2D) \rightarrow N_2^+$ conversion factor from 25–75% and we found that variations in this range did not affect the high-latitude results.

Except for $O^+(^2D)$ we did not take account of metastable ions in our chemical scheme. In a study of the average diurnal variation of the mid-latitude F_1 layer, TORR *et al.* (1979*b*) have shown that the densities of NO^+, O_2^+, N_2^+ and O^+ could be described to within 20–25% by just six photochemical processes; none of these included metastable ions and all of these are included in Table 6. We suspect that the average behavior of the daytime high-latitude F layer can also be described to a good approximation by a relatively simple chemical scheme that does not include all of the metastable chemistry; therefore, the photochemical processes listed in Table 6 are probably more than adequate for our purposes.

Although He^+ is generally in a state of outflow at high-latitudes, we took account of this ion because it might at times significantly influence the N^+ density through the $He^+ + N_2$ reaction. Previous studies by RAITT *et al.* (1978a,b) indicate that outflowing He^+ has a characteristic density profile that exhibits a peak in the 500–700 km altitude range and that possesses a minimum at a higher altitude. In the more recent study, RAITT *et al.* (1978b) calculated He^+ density profiles for several neutral atmospheres, solar EUV fluxes, and geophysical conditions, and it was found that the He^+ peak density can vary by more than a factor of 100 with geophysical

conditions. Additional He^+ density variations occur due to electric field heating and changes in the He^+ escape velocity, but below 800 km these variations are much smaller than those due to changing geophysical conditions [cf. RAITT *et al.*, 1978a). Consequently, the He^+ density profiles calculated by RAITT *et al.* (1978b) for a range of solar cycle, seasonal, and geomagnetic variations were adopted for our model even though they were calculated for slow convection and only one He^+ escape velocity at the upper boundary (0.5 km/sec at 2000 km). The adopted He^+ density profiles are given in Figure 4 of RAITT *et al.* (1978*b*).

5. *Ion Energy Equation*

The ion energy balance is determined by equations (3) and (5). However, for ionospheric applications several simplifications are possible because collisional coupling dominates at low altitudes and because vertical plasma gradients are much more important than horizontal gradients. In particular, at middle and high latitudes, ion stresses arise from relative ion-neutral drifts due to convection electric fields (equation 31). However, because of the large scale-length for horizontal variations, the viscous heating term in equation (3) is much smaller than the ion-neutral frictional heating term in equation (5) and the former can be neglected. Also, the advection and convection terms associated with ion drifts are negligibly small. Therefore, for ionospheric application the ion energy equation reduces to

where the summation in equation (60) is over the electrons and all neutral species. Note that we ignore the small temperature difference between the various ion species and assume a single ion temperature.

For the ion heat flow vector, we adopted the expression derived by CONRAD and SCHUNK (1979) which includes both thermal conduction and diffusion-thermal heat flow. This expression, which was derived for a collision-dominated, partially-ionized, three-component plasma in thermal nonequilibrium, is appropriate at *F*-region altitudes where the dominant species are electrons, O^+ and neutral atomic oxygen. In the magnetic field direction, this expression takes the form,

$$\mathbf{q}_{i\|} = -K'_{ni}\nabla_{\|}T_i - K_{in}\nabla_{\|}T_n + R_{in}(\mathbf{u}_i - \mathbf{u}_n)_{\|} \tag{61}$$

where K'_{ni} and K_{in} are thermal conductivities and R_{in} is the diffusion-thermal coefficient; these expressions are given in Appendix A. Note that ion heat flow is important only in the upper *F*-region where O^+ dominates. Note also that an ion heat flow occurs in response to an ion temperature gradient, a neutral temperature gradient, and a relative ion-neutral drift (diffusion-thermal heat flow).

As with the continuity and momentum equations, if the plasma gradients are in

the vertical direction and the heat flows along **B**, the conductivities in equation (61) must be multiplied by $\sin^2 I$.

6. *Electron Energy Equation*

The electron energy balance can be obtained from equations (3) and (5), but it is more complicated than that found for the ions. First, we note that chemical reactions and viscous heating do not significantly affect the electron energy balance at E and F-region altitudes. Using this fact and the electron continuity equation (1), the electron energy equation can be expressed as

$$\frac{3}{2}n_e k\frac{\partial T_e}{\partial t} = -n_e k T_e(\nabla\cdot\mathbf{u}_e) - \frac{3}{2}n_e k\mathbf{u}_e\cdot\nabla T_e - \nabla\cdot\mathbf{q}_e + \frac{\delta E_e}{\delta t} + Q_e - L_e. \quad (62)$$

Various limiting forms of equation (62) have been used in ionospheric studies over the years (cf. SCHUNK and NAGY, 1978). To obtain a form that is useful for the middle and high-latitude regions of the ionosphere, it is convenient to introduce the electric current, $\mathbf{J}_e$, and the electron heat flow, $\mathbf{q}_e$, (cf. SCHUNK and WALKER, 1970)

$$\mathbf{J}_{e\parallel} = -en_e\mathbf{u}_{e\parallel} \quad (63)$$

$$\mathbf{q}_{e\parallel} = -\beta_e\mathbf{J}_{e\parallel} - K^e\nabla_{\parallel}T_e \quad (64)$$

where β_e is a thermoelectric coefficient and K^e is the electron thermal conductivity. Note that the electric current and heat flow are along the magnetic field. It is also convenient to introduce the Joule heating term, $J_{e\parallel}^2/\sigma_e$, where σ_e is the electrical conductivity. In these expressions, the appropriate conductivities are given by (cf. SCHUNK and WALKER, 1970)

$$\sigma_e = \frac{n_e e^2}{m_e}\frac{1}{\langle v_g\rangle g_{\sigma_0}} \quad (65)$$

$$\beta_e = \frac{5}{2}\frac{kT_e}{e}\frac{g_{\sigma_0}}{g_{\mu_0}} \quad (66)$$

$$K^e = \frac{5n_e k^2 T_e}{m_e}\frac{1}{\langle v_g\rangle}\left[\frac{1}{g_{k_0}} - \frac{g_{\sigma_0}}{2g_{\tau_0}g_{\mu_0}}\right] \quad (67)$$

where $\langle v_g\rangle = \nu_{ei} + \Sigma_n\nu_{en}$ and g_{σ_0}, g_{τ_0}, g_{μ_0} and g_{k_0} are correction factors which account for the variation with velocity of the electron-neutral collision frequency as well as for electron-ion and electron-electron effects. The calculation of the g's is described by SCHUNK and WALKER (1970).

If the gradients of n_e and T_e are primarily in the vertical direction, then the

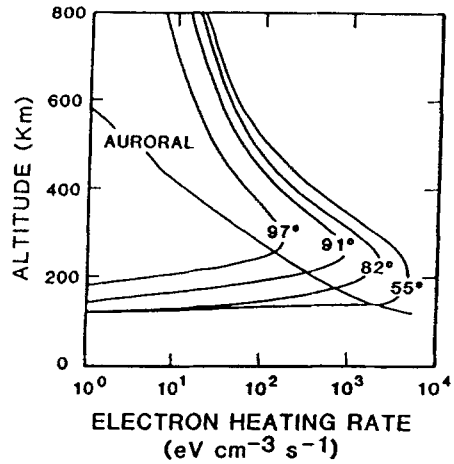

Figure 3
Electron heating rate as a function of altitude for both auroral and solar EUV sources. The auroral heating rate was adopted from REES *et al.* (1971). The EUV heating rate is shown for several solar zenith angles and was calculated using the method described by RICHARDS and TORR (1984).

substitution of equations (63) and (64) into equation (62) yields

$$\frac{3}{2}n_e k\frac{\partial T_e}{\partial t} = \sin^2 I\frac{\partial}{\partial z}\left(K^e\frac{\partial T_e}{\partial z}R\right.$$
$$+ \sin I\frac{kJ_e}{e}\frac{3}{2}\left(1+\frac{5}{3}\frac{g_{\sigma_0}}{g_{\mu_0}}\right)\frac{\partial T_e}{\partial z}$$
$$+ \sin I\frac{kJ_e}{e}\left[\frac{1}{J_e}\frac{\partial J_e}{\partial z}\left(1+\frac{5}{2}\frac{g_{\sigma_0}}{g_{\mu_0}}\right)-\frac{1}{n_e}\frac{\partial n_e}{\partial z}\right]T_e$$
$$+ \frac{J_e^2}{\sigma_e}+\frac{\delta E_e}{\delta t}+Q_e-L_e \qquad (68)$$

where I is the magnetic field dip angle and where the $\|$ sign has been dropped from J_e for convenience. Also, the Joule heating term has been factored out of the $\delta E_e/\delta t$ term so that it is shown explicitly.

In the ionosphere, significant heating occurs in sunlit regions due to photoelectrons and in the auroral oval due to precipitating electrons. For the solar EUV heating rate, we adopted the model of Richards (private communication, 1984) and RICHARDS and TORR, (1984). This model computes the thermal electron volume heating rate as a by-product of the EUV-produced photoelectron flux. For the auroral heating rate, we adopted the profile computed by REES *et al.* (1971), but the profile is scaled according to the auroral electron energy flux. Figure 3 shows representative heating rate profiles for different solar zenith angles. These profiles lie along the noon meridian and correspond to solar maximum and winter conditions in the northern

hemisphere. A characteristic feature of these profiles is the decrease in the peak heating rate as the solar zenith angle increases, particularly near the terminator. Also shown in Figure 3 is the thermal electron heating rate due to precipitating auroral electrons with an energy flux of 1 erg cm^{-2} s^{-1}. This heating rate displays a marked exponential decrease with altitude because we assumed that the precipitating electron spectrum was hard (several keV).

There are a number of processes that are effective in cooling the electron gas. In the lower *F*-region, where the molecular species are abundant, rotational excitation of N_2 and O_2 and excitation of the fine structure levels of atomic oxygen are the most important cooling processes. However, at electron temperatures greater than 1500°K, vibrational excitation of N_2 and O_2 and electronic excitation of O and O_2 have to be considered. At high altitudes, Coulomb collisions with the ambient ions are an important energy loss mechanism for thermal electrons, and in some cases elastic collisions with the ambient neutrals have to be considered.

For electron cooling due to inelastic collisions, we adopted the following expressions:

$$L(e, N_2)_{rot} = 2.9 \times 10^{-14} n_e n(N_2)(T_e - T_n)/T_e^{1/2} \tag{69}$$

$$L(e, O_2)_{rot} = 6.9 \times 10^{-14} n_e n(O_2)(T_e - T_n)/T_e^{1/2} \tag{70}$$

$$L(e, N_2)_{vib} = 2.99 \times 10^{-12} n_e n(N_2) \exp[f(T_e - 2000)/2000T_e] \cdot \left[\exp\left(-g\frac{T_e - T_n}{T_e T_n}\right) - 1\right] \tag{71}$$

$$L(e, O_2)_{vib} = 5.2 \times 10^{-13} n_e n(O_2) \exp[h(T_e - 700)/700T_e] \cdot \left[\exp\left(-2770\frac{T_e - T_n}{T_e T_n}\right) - 1\right] \tag{72}$$

$$L(e, O(^1D)) = 1.57 \times 10^{-12} n_e n(O) \exp\left(d\frac{T_e - 3000}{3000T_e}\right) \cdot \left[\exp\left(-22713\frac{T_e - T_n}{T_e T_n}\right) - 1\right] \tag{73}$$

$$L(e, O)_f = 8.629 \times 10^{-6} \frac{n_e n(O)}{Z} \sum A(B!) T_e^{(B-1/2)} \{\varepsilon(D_x - E_x) + 5.91 \times 10^{-9}(T_n - T_e)[(1 + B)D_x + (E/T_e + 1 + B)E_x]\} \tag{74}$$

where

$$f = 1.06 \times 10^4 + 7.51 \times 10^3 \tanh[1.10 \times 10^{-3}(T_e - 1800)] \tag{75}$$

$$g = 3300 + 1.233(T_e - 1000) - 2.056 \times 10^{-4}(T_e - 1000)(T_e - 4000) \quad (76)$$

$$h = 3300 - 839 \sin[1.91 \times 10^{-4}(T_e - 2700)] \quad (77)$$

$$d = 2.4 \times 10^4 + 0.3(T_e - 1500) - 1.947 \times 10^{-5}(T_e - 1500)(T_e - 4000), \quad (78)$$

and where for the fine structure cooling rate the additional parameters are defined as follows: $B!$ is B factorial,

$$Z = 5 + 3\exp(-228/T_1) + \exp(-326/T_0), \quad (79)$$

T_0 is the temperature of the $J = 0$ level and T_1 is the temperature of the $J = 1$ level. The summation in equation (74) is over the three transitions 1–2, 0–2, and 0–1 and in respective order the other parameters in equation (74) are

$$\varepsilon = 0.02; 0.028; 0.008 \quad (80)$$

$$D_x = \exp(-228/T_i); \exp(-326/T_0); \exp(-326/T_0) \quad (81)$$

$$E_x = \exp(-228/T_e); \exp(-326/T_e); \exp\left[-\left(\frac{98}{T_e} + \frac{228}{T_1}\right)\right] \quad (82)$$

$$E = 228; 326; 98 \quad (83)$$

$$A = 8.58 \times 10^{-6}; 7.201 \times 10^{-6}; 2.463 \times 10^{-7} \quad (84)$$

$$B! = 1.008; 0.9617; 1.1448. \quad (85)$$

In the thermal electron cooling rate expressions, the units are eV cm^{-3} s^{-1}. These rates were taken from the following sources: N_2 rotation (DALGARNO, 1968); O_2 rotation (DALGARNO, 1968); N_2 vibration (STUBBE and VARNUM, 1972); O_2 vibration (PRASAD and FURMAN, 1973); O fine structure (HOEGY, 1976); and O($'D$) (HENRY *et al.*, 1969).

The electron-neutral cooling rates due to elastic collisions are obtained from equation (5) using the momentum transfer cross-sections given in Table 1. Specifically, these cooling rates are given by

$$L(e, N_2) = 1.77 \times 10^{-19} n_e n(N_2)[1 - 1.21 \times 10^{-4} T_e] T_e(T_e - T_n) \quad (86)$$

$$L(e, O_2) = 1.21 \times 10^{-18} n_e n(O_2)[1 + 3.6 \times 10^{-2} T_e^{1/2}] T_e^{1/2}(T_e - T_n) \quad (87)$$

$$L(e, O) = 7.9 \times 10^{-19} n_e n(O)[1 + 5.7 \times 10^{-4} T_e] T_e^{1/2}(T_e - T_n) \quad (88)$$

$$L(e, He) = 2.46 \times 10^{-17} n_e n(He) T_e^{1/2}(T_e - T_n) \quad (89)$$

$$L(e, H) = 9.63 \times 10^{-16} n_e n(H)[1 - 1.35 \times 10^{-4} T_e] T_e^{1/2}(T_e - T_n) \quad (90)$$

where the units are eV cm^{-3} sec^{-1}.

The energy transfer rate for electron-ion interactions can be obtained from equations (5) and (7). If the different ion species are assumed to have a common

temperature, the electron cooling rate for a mixture of ions is given by

$$L(e, i) = 3.2 \times 10^{-8} n_e \frac{(T_e - T_i)}{T_e^{3/2}} \ln \Lambda [n(O^+) + 4n(He^+) + 16n(H^+) + 0.50n(O_2^+) + 0.53n(NO^+)] \quad (91)$$

where the units are eV cm^{-3} s^{-1} and $\ln \Lambda$ is the Coulomb logarithm.

7. *Numerical Solution*

Because there are different time scales governing the ion densities, the ion temperature and the electron temperature, it is not necessary to solve all of the equations simultaneously at each time step. Also, the minor ion diffusion equations do not have to be solved simultaneously with the major ion diffusion equations. The procedure we adopted is described in the following paragraphs.

7.1. *Major Ion Densities*

The equations describing the major ion densities are obtained by substituting the ion momentum equations (29) into the ion continuity equations (25). This procedure yields a set of coupled, nonlinear, second order, parabolic partial differential equations of the form

$$\frac{\partial n_i}{\partial t} = A_{1i}(z, t) \frac{\partial^2 n_i}{\partial z^2} + A_{2i}\left(z, t, n_e, \frac{\partial n_e}{\partial z}\right) \frac{\partial n_i}{\partial z} + A_{3i}\left(z, t, n_e, \frac{\partial n_e}{\partial z}, \frac{\partial^2 n_e}{\partial z^2}\right) n_i + A_{4i}(z, t, n_j) \quad (92)$$

where subscript j corresponds to another ion species. In our model, equations of the form of (92) were solved for NO^+, O_2^+, and O^+. For N_2^+, the chemical lifetime is so short that we can assume chemical equilibrium at all times of the day and at all altitudes,

$$n(N_2^+) = P'(N_2^+)/L'(N_2^+). \quad (93)$$

The electron density is then given as a sum of the major ion densities,

$$n_e = n(NO^+) + n(O_2^+) + n(N_2^+) + n(O^+). \quad (94)$$

At this point, the set of ion equations (92) are linearized in time. That is, all ion-ion and ion-electron coupling terms are expanded in a Taylor series. For a coupling term f, the expansion is

$$f(t + \Delta t) = f(t) + (df/dt)\Delta t + \ldots \quad (95)$$

For example, if we let subscripts 1, 2, and 3 correspond to NO^+, O_2^+, and O^+ respectively, and consider the coupling term

$$f(t) = n_1 n_e \tag{96}$$

then

$$f(t + \Delta t) = (n_e + n_1)^t n_1^{t+\Delta t} + n_1^t n_2^{t+\Delta t} + n_1^t n_3^{t+\Delta t} - n_e^t n_1^t . \tag{97}$$

After a considerable amount of algebra, equation (92) for a given ion species becomes linear in time, but it contains spatial derivatives for all of the ion species that exhibit field-aligned diffusion. For example, for NO^+ (subscript 1), equation (92) becomes

$$\begin{aligned}\frac{\partial n_1}{\partial t} = {} & G_1 \frac{\partial^2 n_1^{t+\Delta t}}{\partial z^2} + G_2 \frac{\partial n_1^{t+\Delta t}}{\partial z} + G_3 n_1^{t+\Delta t} \\ & + G_4 \frac{\partial^2 n_2^{t+\Delta t}}{\partial z^2} + G_5 \frac{\partial n_2^{t+\Delta t}}{\partial z} + G_6 n_2^{t+\Delta t} \\ & + G_4 \frac{\partial^2 n_3^{t+\Delta t}}{\partial z^2} + G_5 \frac{\partial n_3^{t+\Delta t}}{\partial z} + G_7 n_3^{t+\Delta t} + G_8\end{aligned} \tag{98}$$

where the G-coefficients are complicated expressions, but they are calculated at time t. Similar equations exist for O_2^+ and O^+, and all three must be solved simultaneously.

The next step is to obtain finite differences for the spatial and temperal derivatives. We adopted space-centered spatial derivatives and forward time derivatives. Letting n be one of the densities and α correspond to the spatial index, the adopted expressions are

$$\frac{\partial n}{\partial t} = \frac{n_\alpha^{t+\Delta t} - n_\alpha^t}{\Delta t} \tag{99}$$

$$\frac{\partial^2 n}{\partial z^2} = \frac{n_{\alpha+1} - 2n_\alpha + n_{\alpha-1}}{(\Delta z)^2} \tag{100}$$

$$\frac{\partial n}{\partial z} = \frac{n_{\alpha+1} - n_{\alpha-1}}{2(\Delta z)} \tag{101}$$

where equations (100) and (101) hold for times t and $t + \Delta t$. These finite-difference derivatives convert the set of partial differential equations for the major ions of the form (98) into a set of algebraic equations, which can be solved by standard tridiagonal matrix techniques (cf. CRANK and NICOLSON, 1947).

With regard to boundary conditions, we take account of the fact that field-aligned diffusion is negligible at the lower boundary and obtain the ion densities there by equating local production and loss rates. At the upper boundary, we assume that the fluxes of NO^+ and O_2^+ are negligibly small. The flux of O^+ through the upper

boundary can be obtained by integrating the O^+ continuity equation from the top boundary, z_T, to infinity (STROBEL and MCELROY, 1970)

$$[n(O^+)u(O^+)]_{z_T} = [n(O^+)u(O^+)]_\infty - [H(O)P'(O^+)]_{z_T} + \frac{\partial}{\partial t}[H(O^+)n(O^+)]_{z_T} \tag{102}$$

where

$$H(O) = kT_n/m(O)g \tag{103}$$

$$H(O^+) = k(T_e + T_i)/m(O^+)g \tag{104}$$

and where the first term on the right-hand side of equation (102) corresponds to the O^+ flux that escapes from the ionosphere.

In the model, we do not 'directly' take into account interhemispheric flow along closed field lines. Under certain circumstances, this interhemispheric flow can be an important maintenance process for the nocturnal *F*-region at mid-latitudes (e.g., BAILEY *et al.*, 1978; CHANDLER *et al.*, 1983; MOFFETT *et al.*, 1986). A downflow of H^+ from the outer plasmasphere will be converted into an O^+ downflow because of the charge exchange reaction $H^+ + O \rightleftharpoons O^+ + H$. Such a flow enters our model via the first term on the right-hand-side of equation (102).

7.2. *Minor Ion Densities*

The equations describing the minor ion densities are obtained by substituting the minor ion momentum equation (36) into the continuity equation (25). The resulting equation is a second order, parabolic, partial differential equation similar to the major ion equation (92). However, because the electron density is determined by the major ions, the minor ion diffusion equation is basically linear and of the form

$$\frac{\partial n_j}{\partial t} = B_{1j}(z, t)\frac{\partial^2 n_j}{\partial z^2} + B_{2j}(z, t)\frac{\partial n_j}{\partial z} + B_{3j}(z, t)n_j + B_{4j}(z, t) \tag{105}$$

where the subscript j corresponds to a minor ion species and where the *B*-coefficients depend on the major ions and electrons. The derivatives in equation (105) can be eliminated with finite difference expressions (equations 99–101) and the resulting set of linear algebraic equations can be solved with standard tridiagonal matrix inversion techniques (CRANK and NICHOLSON, 1947). Note that the equations for the different minor ion species can be solved separately, since the different minor ion species are not coupled to each other. With regard to boundary conditions, we used the fact that diffusion is negligible at the lower boundary and obtained the minor ion densities there by equating local production and loss rates. We also specified the flux of minor ions through the upper boundary. For N^+, this flux was taken to be zero.

7.3. *Ion and Electron Temperatures*

A single equation describing the ion temperature can be obtained by substituting the ion heat flow expression (61) into the ion energy equation (60). Likewise, a similar equation for the electron temperature can be obtained by substituting equation (67) into the electron energy equation (68). Both of these equations are nonlinear, second order, parabolic, partial differential equations, and therefore, they need to be linearized in time before finite difference expressions are introduced for the derivatives. However, first, it is convenient to introduce a change of variables for both T_e and T_i; namely, $\theta = T^{7/2}$. With this change of variables, the equations for both T_e and T_i take the form

$$\frac{\partial \theta}{\partial t} = A_1(z, t)\frac{\partial^2 \theta}{\partial z^2} + A_2(\theta, z, t)\frac{\partial \theta}{\partial z} + A_3(\theta, z, t)\theta + A_4(\theta, z, t). \tag{106}$$

The terms that are nonlinear in θ are then linearized in time in the manner described earlier and the resulting linear equations are solved via the standard tridiagonal technique. For boundary conditions, we specify the heat conducted through the upper boundary, and at the lower boundary we equate local heating and cooling rates since thermal conduction is not important at low altitudes.

7.4. *Integration Procedure*

As the density and temperature equations are integrated forward in time, the ordering is as follows. At a given time step Δt, we first obtain a simultaneous solution of the major ion diffusion equations (92) and (93), which yields the ion densities for NO^+, O_2^+, N_2^+, and O^+. Next, the electron density is determined via equation (94). Then, the minor ion densities are obtained from separate solutions of equations similar to (105), and finally, the electron and ion temperatures are obtained from solutions of equations of the form (106). At this point, time is advanced by Δt and the procedure is repeated.

8. *Model Inputs*

As noted earlier, several input parameters are needed by our ionospheric model, including a neutral atmosphere, a thermospheric wind pattern, a plasma convection pattern, and an auroral oval. In what follows, we will give representative examples of the important input parameters.

8.1. *Neutral Atmosphere*

For the atmospheric densities and temperature, we generally adopt the mass spectrometer and incoherent scatter (MSIS) model developed by HEDIN *et al.*

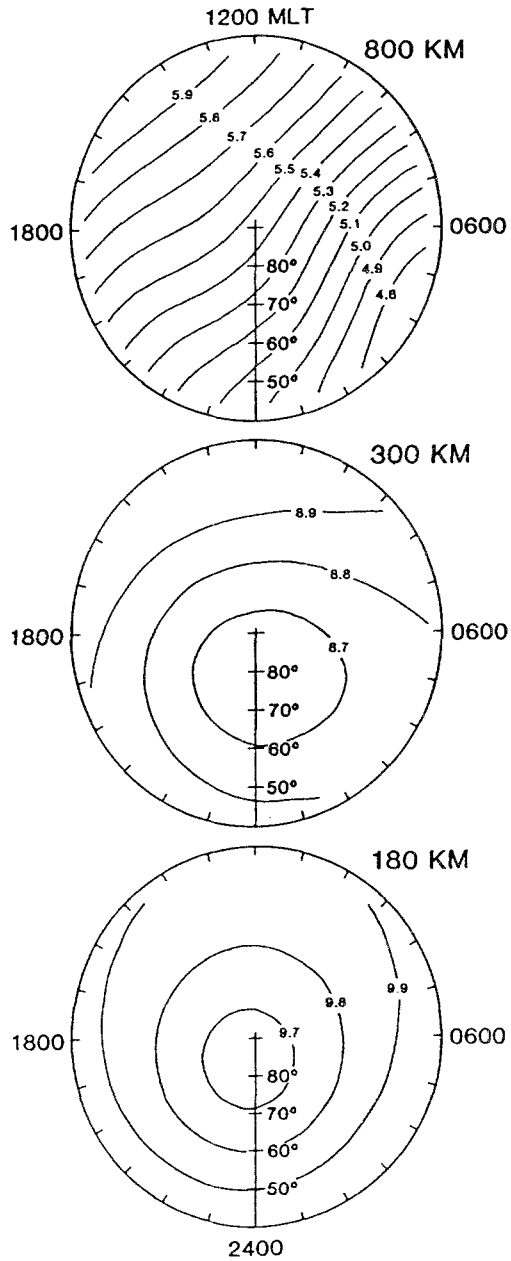

Figure 4
Contours of $\log_{10}[O]$ as a function of magnetic latitude and MLT at three altitudes for 1700 UT. The densities (cm^{-3}) were obtained from the MSIS atmospheric model (HEDIN *et al.*, 1977a,b).

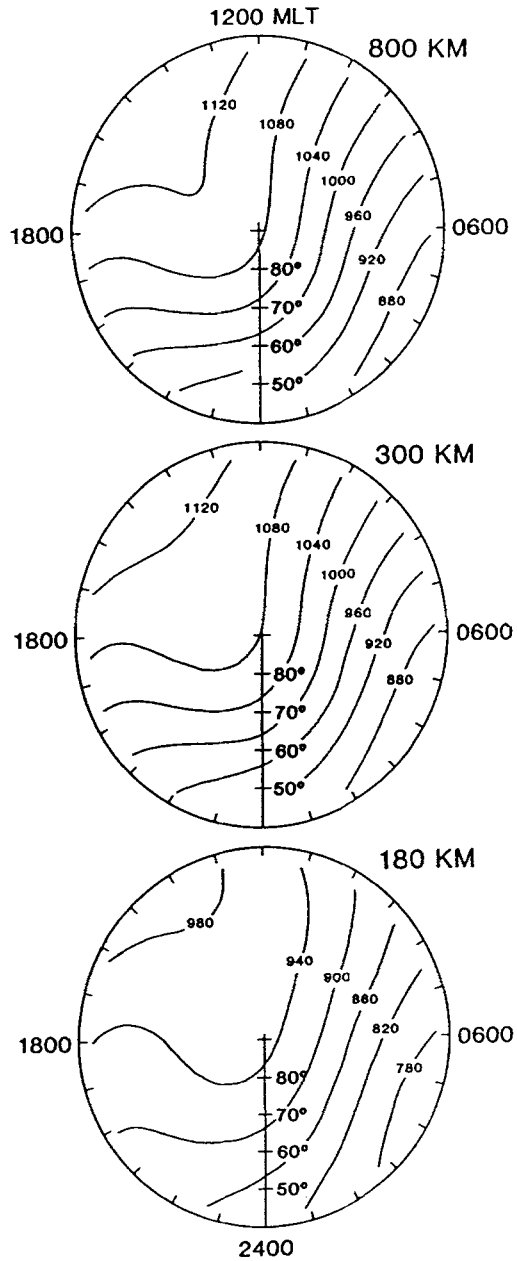

Figure 5
Contours of neutral temperature as a function of magnetic latitude and MLT at three altitudes for 1700 UT. The temperatures (°K) were obtained from the MSIS atmospheric model (HEDIN *et al.*, 1977a,b).

(1977a,b). Representative atomic oxygen densities are shown in Figure 4 at three altitudes for solar maximum ($F_{10.7} = 150 \times 10^{-22}$ Wm^{-2} Hz^{-1}) and strong geomagnetic activity ($Ap = 35$) conditions. At low altitudes, below 300 km, the density has a minimum near the magnetic pole and varies by only a factor of two between 50° and the pole. In sharp contrast, at high altitudes (top panel) the density has a maximum at low latitudes around 1500 MLT and decreases by over an order of magnitude across the polar cap to 50° at 0400 MLT. The density decreases exponentially with altitude with a scale height that depends on the neutral temperature.

Figure 5 shows the neutral temperature plotted in the same format as Figure 4 for the same altitudes and UT. At all three altitudes, T_n has a maximum at low latitudes around 1500 MLT and decreases over the pole to a minimum around 0500 MLT. This variation is similar to that of [O] at high altitudes owing to the scale height dependence of [O] above 300 km. T_n varies by about 200 K across the high latitude ionosphere, with a maximum value of about 1120 K. Above 300 km, T_n is essentially constant with altitude.

8.2. Thermospheric Wind Pattern

For our neutral wind pattern, we generally fit an analytical expression for the wind to that deduced from incoherent scatter radar data. For the analytical expression, we adopted a modified form of the thermospheric wind pattern given by MURPHY *et al.* (1976). Figure 6 shows contours of a representative meridional neutral wind at two universal times. The wind blows away from the subsolar point, and consequently, blows poleward on the dayside and equatorward at night on the noon-midnight meridian. The adopted wind has north-south symmetry in a frame whose equatorial plane contains the subsolar direction, but the local time symmetry axis is moved from the noon-midnight to the 1300–0100 LT meridian plane. Only the meridional wind component is shown in Figure 6; it is zero on this equator and increases sinusoidally with latitude to a maximum value at 30° from this equator. Poleward of this location the wind is constant with latitude. The local time variation of this meridional wind is a cosine function with a maximum poleward wind of 50 m/s at 1300 LT and a maximum equatorward wind of 200 m/s at 0100 LT. At the terminator (the poles in this subsolar frame), the meridional wind increases smoothly from the lower dayside value to its nightside value over 20° of latitude.

8.3. Plasma Convection Pattern

The plasma convention pattern induced by magnetospheric electric fields has been extensively studied during the last two decades and several empirical models describing the pattern have been developed (VOLLAND, 1978; HEPPNER, 1977; FOSTER, 1983; HEELIS *et al.*, 1982; SOJKA *et al.*, 1986). The convection pattern displays a marked variation with the interplanetary magnetic field (IMF), and for southward

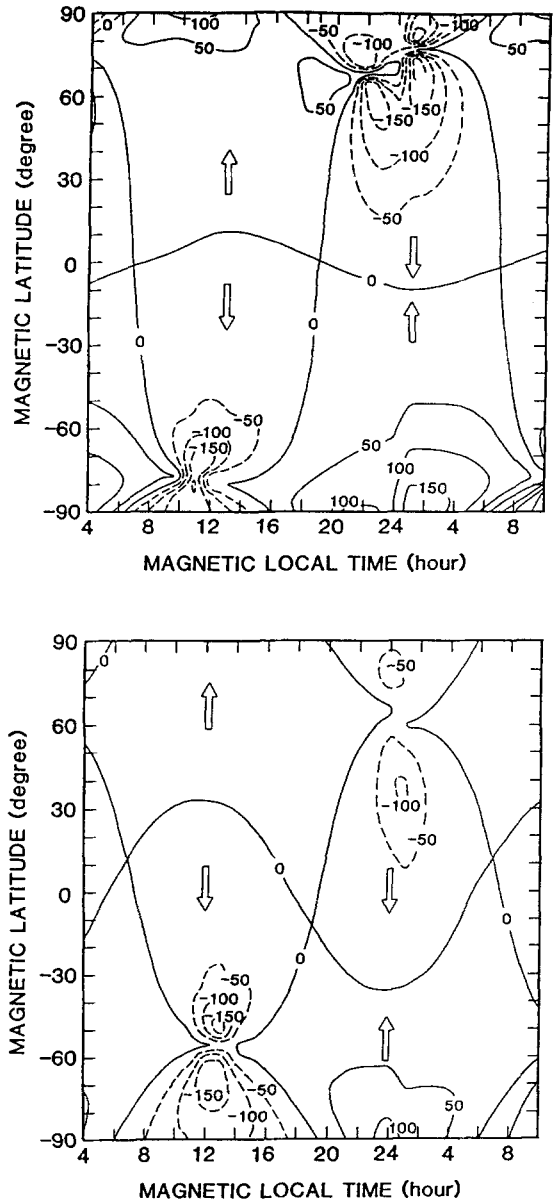

Figure 6
Contours of the meridional neutral wind at 0300 UT (top panel) and 1500 UT (bottom panel) displayed in a magnetic dipole coordinate system. The contours are labeled in meters per second with positive values corresponding to a wind direction from south to north. The arrows highlight the flow pattern. From SOJKA and SCHUNK (1985).

IMF the pattern has two vortex cells with antisunward flow over the polar cap and return flow equatorward of the auroral oval. For northward IMF, on the other hand, the convection pattern is either irregular or it contains a multi-cell structure with sunward flow in the polar cap. The effect of a B_y component of the IMF is basically to produce asymmetric convection cells. In addition to the magnetospheric-driven flow, the high-latitude ionosphere also has a tendency to corotate with the earth.

Figure 7*a* shows a representative two-cell convection pattern with corotation added. In this figure, ten plasma drift trajectories are shown for an asymmetric magnetospheric electric field pattern with enhanced plasma flow in the dusk sector of the polar region. The total cross-tail potential is 90 kV, which roughly corresponds to a *Kp* of 5. Also shown in Figure 7*a* is a representative auroral oval. Field tubes of plasma following trajectories 1 and 2 appear to corotate; however, only trajectory 1 corresponds to corotation. Field tubes following trajectory 2 take 1.35 days to complete a full circulation owing to speed variations along the path. Field tubes of plasma following trajectories 3 and 4 execute motions which result in a reversal of corotation in the afternoon sector. Field tubes following trajectories 5, 6 and 7 form a dawn cell rotating in a corotational sense, while field tubes following trajectories 8, 9 and 10 rotate in a counter corotation sense. In the centers of these two cells the

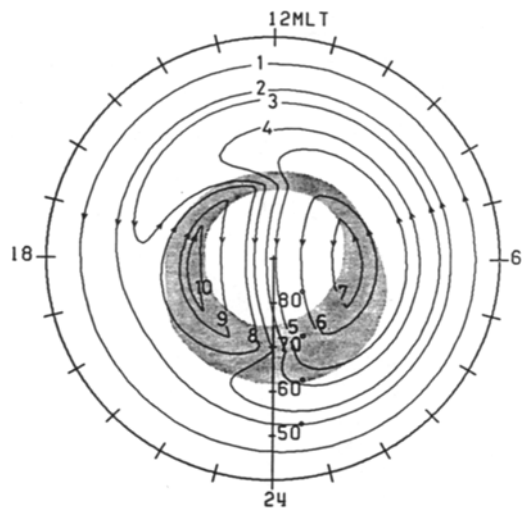

LABEL	1	2	3	4	5	6	7	8	9	10
PERIOD (DAY)	1.06	1.35	1.32	0.79	0.58	0.25	0.15	0.27	0.11	0.06

Figure 7*a*

Plasma drift trajectories in the magnetic quasi-inertial frame for a cross-tail magnetospheric electric potential of 90 kV. The shaded region corresponds to an auroral oval for $K_p = 5$. Magnetic local time (MLT) is indicated by tick marks at hourly intervals and magnetic latitude is indicated on the vertical scale. The trajectories have been numbered in order to indicate circulation times, which are tabulated in the lower part of the figure (from SOJKA *et al.*, 1981b).

plasma circulates extremely rapidly; 0.15 days for trajectory 7 and 0.06 days for trajectory 10. An evening sector stagnation region is present in an extended region from 1800 to 2200 MLT and from 58° to 62° latitude.

A cross-tail potential of 90 kV is fairly large, and therefore, large plasma convection velocities can be expected in certain regions of the high-latitude ionosphere. This is shown in Figure 7*b*, where contours of the horizontal plasma convection speed are plotted in the magnetic quasi-inertial frame. Each contour is labeled with its appropriate speed in m/s; the region with speeds below 100 m/s is indicated by the shading. A region of high speed, reaching almost 2 km/s, is located in the dusk sector and it corresponds to the enhanced magnetospheric electric field on the dusk side of the polar ionosphere. Over the polar cap the horizontal speed lies in the 200 to 600 m/s range. In contrast, an extended low-speed region is present in the afternoon and evening sectors. The location of this extended low-speed region has a direct bearing on the location of the main or mid-latitude plasma density trough.

Since the geomagnetic field lines at high latitudes are not completely vertical, an $\mathbf{E} \times \mathbf{B}$ plasma motion will have a vertical component. Figure 7*c* shows contours of the vertical component of the plasma convection velocity in the magnetic quasi-inertial frame. Each contour is labeled with the appropriate velocity in m/s; the dashed contours represent downward velocities, while the solid contours represent upward velocities. Upward electrodynamic drifts occur on the dayside where the plasma is convecting toward the magnetic pole, while downward electrodynamic drifts occur in the nightside where the plasma is convecting away from the magnetic pole. For the case considered, the vertical plasma drift ranges from $+50$ m/s to -70

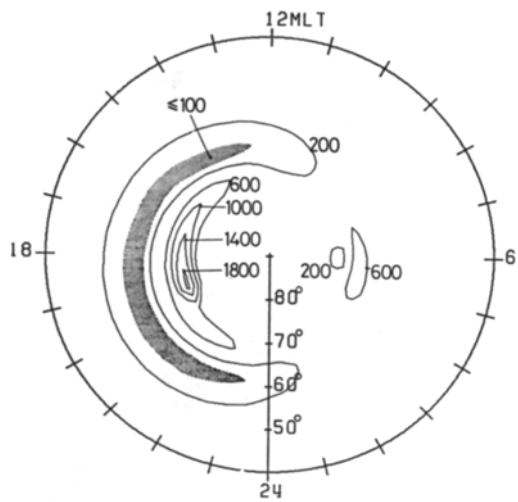

Figure 7*b*

Contours of horizontal plasma drift speeds in the magnetic quasi-inertial frame. The contours are labeled in units of m s^{-1} and the shaded region corresponds to speeds below 100 m s^{-1} (from Sojka *et al.*, 1981b).

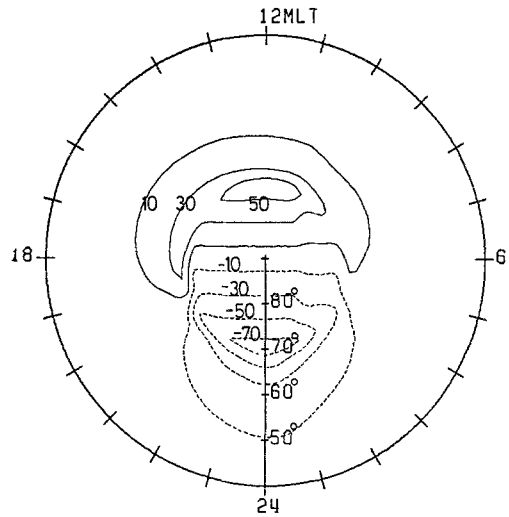

Figure 7*c*
Contours of the vertical component of the electrodynamic plasma drift velocity displayed in the magnetic quasi-inertial frame. The solid contours correspond to upward drift and the dashed contours correspond to downward drift. The contours are labeled in units of m s^{-1} (from SOJKA *et al.*, 1981b).

m/s. Vertical drifts near the extremes of this range have a pronounced effect on both the *F*-region peak electron density, N_mF_2, and the altitude of the peak, h_mF_2.

The convection pattern shown in Figures 7*a–c* is the one seen in the magnetic reference frame. Because of the displacement between the geographic and geomagnetic poles, this pattern rotates about the geographic pole while continually pointing toward the sun. Therefore, the high latitude ionosphere moves toward and then away from the sun during the course of a day. This motion introduces a universal time dependence in the photoionization rate, and hence, electron density.

8.4. Auroral Oval

Particle precipitation in the auroral oval acts as an ionization source, a source of bulk heating for the electron gas, and a thermal conduction source through our upper boundary. At the present time, there are several empirical models that describe the precipitating electron energy flux and characteristic energy (FELDSTEIN and STARKOV, 1967; SPIRO *et al.*, 1982; WALLIS and BUDZINSKI, 1981). The simple auroral oval shown in Figure 7*a* corresponds to a FELDSTEIN and STARKOV (1967) auroral oval for $Kp = 5$ conditions and for a precipitating electron energy flux of 1 erg cm^{-2} s^{-1}. This auroral oval was used in a model study that will be presented in the next section.

9. *Model Densities and Temperatures*

The mid-high latitude ionospheric model described in the previous sections has been used extensively during the last decade in a variety of applications. The model has been used to elucidate the physical and chemical processes governing the formation of ionospheric features, such as the polar ionization hole, the cross polar cap tongue of ionization, the main electron density trough, ion and electron temperature hot spots, and plasma blobs. The model has also been used to study the temporal response of the ionosphere to stormtime dynamics and has been tested against both satellite and incoherent scatter radar data. Some of these applications have been briefly reviewed in recent conference proceedings (SCHUNK, 1983; SCHUNK, 1987; SCHUNK and SOJKA, 1987; SOJKA and SCHUNK, 1987), and a comprehensive review of the applications of the ionospheric model is in progress (Sojka, private communication, 1987). Here, we merely want to display some recent results which exhibit the full capabilities of the model.

Several interesting ionospheric features were produced in a recent study pertaining to solar maximum, winter solstice, and strong geomagnetic activity conditions. The convection and particle precipitation patterns adopted for this study are the ones shown in Figures 7*a–c*, and the adopted thermospheric density, temperature, and wind distributions are shown in Figures 4–6. The resulting ionospheric response to these inputs was calculated using the 3-dimensional, time-dependent ionospheric model (SCHUNK *et al.*, 1986).

Figure 8 shows contours of $\log_{10} N_e$ at three altitudes for 1700 UT. At this UT, more of the polar cap is sunlit than at any other time of the day; the terminator extends from 1800 to 0700 MLT. At 180 km N_e reflects the balance between production and loss with both the auroral oval and terminator being discernible via the gradients in density. The auroral oval is a region where the density is about 10^5 cm^{-3}, while the terminator is a region where the density decreases smoothly from 10^5 to below 5×10^3 cm^{-3}. At this altitude the density varies by more than two orders of magnitude.

The N_e variation at 300 km is considerably more complex. The highest densities are still associated with the oval and sunlight, but transport effects have smeared these regions. A region of high density has been transported into the polar cap from the dayside, producing a 'tongue of ionization'. In the evening-midnight-morning sector equatorward of the oval, the 'mid-latitude trough' is well defined. The increase in density equatorward of the trough is due to the upward plasma drift induced by the neutral wind. Note that in the evening sector the mid-latitude trough extends across the terminator (1800 MLT) and into sunlight. Such a situation only occurs at this UT, and as will be shown later, produces an interesting T_e effect. At 800 km, plasma transport is even more important than at 300 km and the various *F*-region features are not as distinct.

The ion temperatures that are associated with the electron densities in Figure 8

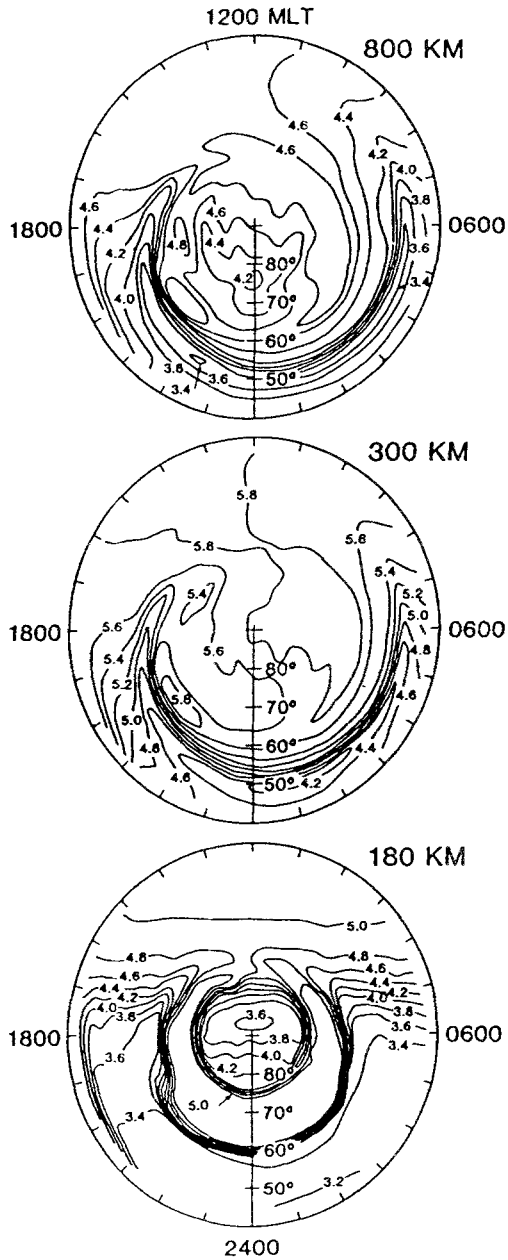

Figure 8
Contours of $\log_{10} N_e$ (cm^{-3}) as a function of magnetic latitude and MLT at three altitudes for 1700 UT. From SCHUNK *et al.* (1986).

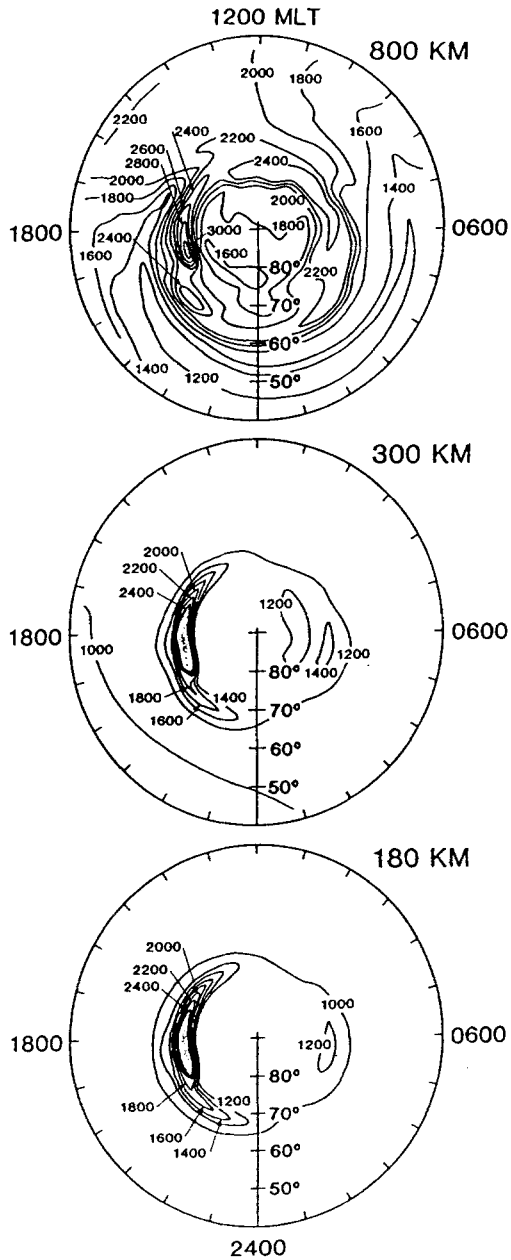

Figure 9
Contours of ion temperature (K) as a function of magnetic latitude and MLT at three altitudes for 1700 UT. From SCHUNK *et al.* (1986).

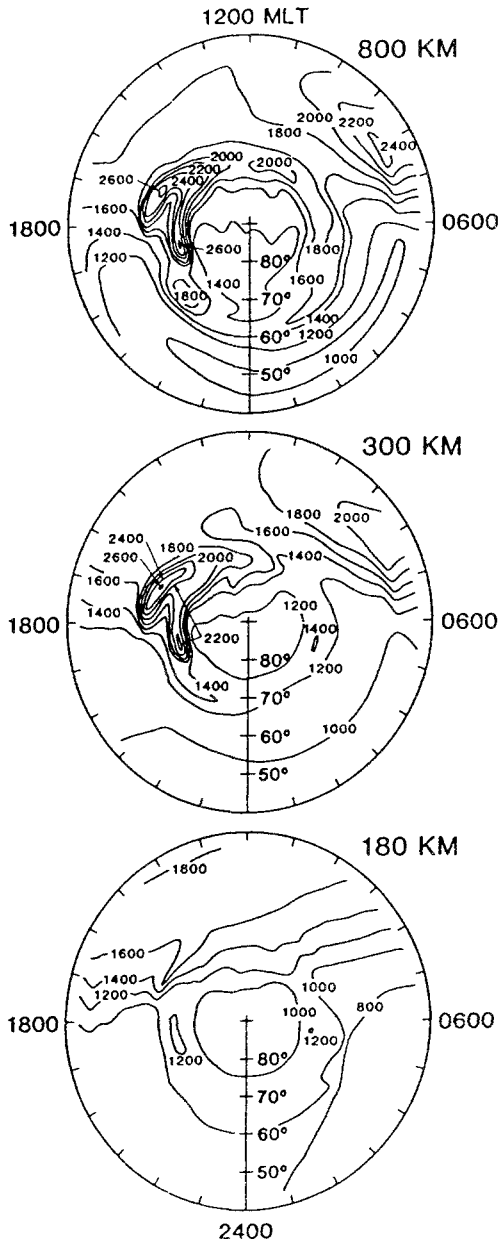

Figure 10
Contours of electron temperature (K) as a function of magnetic latitude and MLT at three altitudes for 1700 UT. For these calculations the electron heat flux through the upper boundary was zero. From SCHUNK *et al.* (1986).

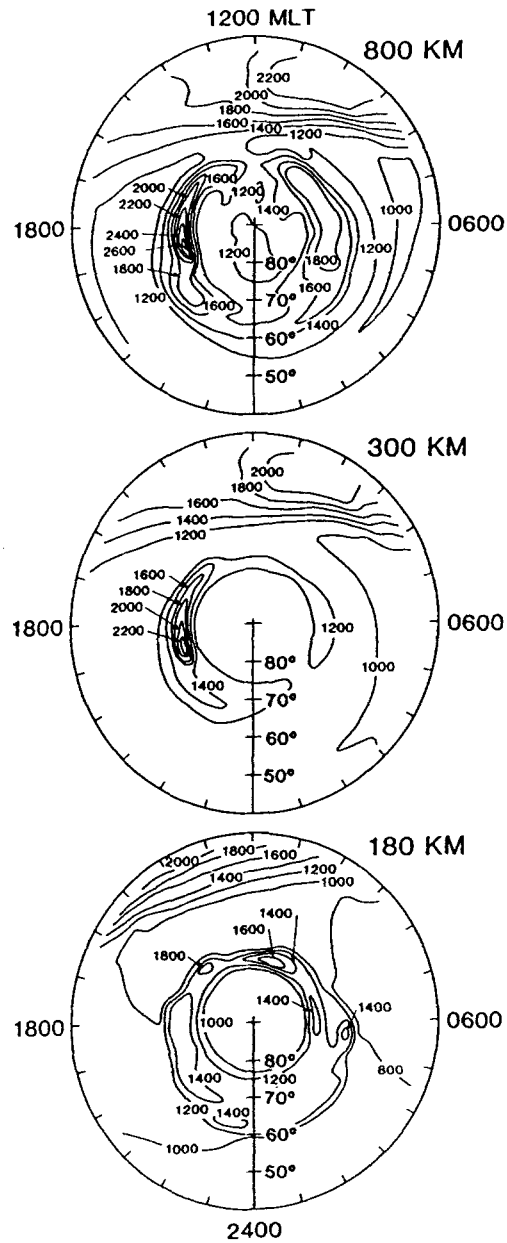

Figure 11
Contours of electron temperature (K) as a function of magnetic latitude and MLT at three altitudes for 0500 UT. For these calculations the electron heat flux through the upper boundary was zero. From SCHUNK *et al.* (1986).

are shown in Figure 9. At both 180 and 300 km, the ion temperature exhibits very little solar control, and the ion energy balance is mainly determined by ion-neutral interactions. Because of the high electric fields in the dusk sector, an ion 'hot spot' is generated. This 'hot spot' results from the ion-neutral frictional heating in the region of high electric fields. At low altitudes, this heating mechanism produces ion temperatures that are more than double the neutral temperatures; T_i reaches 2600 K in the center of the 'hot spot' at 300 km. The T_i distribution is relatively complicated at 800 km, since it depends upon three inputs; neutral density, T_n and N_e. A full description of the ion 'hot spot' as well as the UT variations of T_i is given by SCHUNK *et al.* (1986).

The electron temperatures that are consistent with the electron densities and ion temperatures displayed in Figures 8 and 9 are shown in Figure 10. At 180 km, the electron temperature is strongly controlled by local heating and cooling processes. On the dayside, T_e decreases with increasing solar zenith angle from a high of about 1800 K to a low of about 800 K. Elevated electron temperatures exist in the auroral oval owing to heating from precipitating electrons, but T_e is higher in sunlight than in the auroral oval by about 600 K at this UT. Note that at 1700 UT the elevated electron temperatures on the dayside merge with those in the auroral oval (terminator crosses auroral oval).

At and above 300 km, T_e still has the same auroral oval and dayside features as at 180 km. However, at these higher altitudes, two electron temperature 'hot spots' appear in the dusk sector. The electron temperature hot spot at 70° latitude and 1800 MLT coincides with the location of the ion temperature hot spot (see Figure 9). In this region, the ions are hotter than the electrons and they transfer heat to the electrons via Coulomb collisions, raising their temperature to 2200 K in the center of the hot spot at 300 km. The second T_e hot spot at 65° latitude and 1600 MLT is a region where $T_e > T_i$ and where T_e reaches 2600 K. This hot spot coincides with the extension of the mid-latitude trough across the terminator and into sunlight, as noted earlier in connection with Figure 8. As the low electron densities in the trough convect into sunlight, T_e increases rapidly owing to the short time constant for heating, while the N_e buildup takes much longer. At later times, when the terminator moves to lower latitudes, the trough segment that extends to 1600 MLT in the dusk sector is not sunlit, and consequently, the second T_e hot spot disappears (see Figure 11).

As a final example of the model's capabilities, we show the effect of ionospheric return currents on auroral electron temperatures. An electron heat flow can occur in a partially-ionized plasma in response to either an electron temperature gradient (thermal conduction) or an electron current (thermoelectric heat flow). The former process has been extensively studied, while the latter process has received relatively little attention. Therefore, we used our time-dependent three-dimensional model of the high-latitude ionosphere to study the effect of field-aligned ionospheric return currents on auroral electron temperatures for different seasonal and solar cycle conditions as well as for different heat fluxes at our upper boundary (800 km).

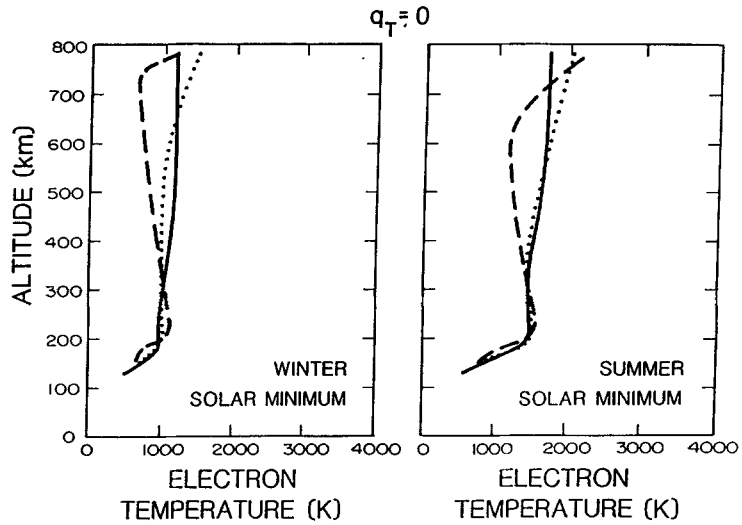

Figure 12
Electron temperature profiles in the nocturnal auroral oval for three values of the field-aligned return current at solar minimum for both summer and winter conditions. The field-aligned current values are 0 (solid curves), -1×10^{-5} (dotted curves) and -5×10^{-5} (dashed curves) amp m^{-2}. From SCHUNK *et al.* (1987).

Figure 12 shows electron temperature profiles for three values of the field-aligned return current for summer and winter conditions at solar minimum. The field-aligned currents are 0 (solid curves), -1×10^{-5} (dotted curves), and -5×10^{-5} (dashed curves) amp m^{-2}. The profiles were calculated with the total heat flow through the upper boundary set to zero. The solid curves correspond to the typical case of no field-aligned current and no heat flow through the upper boundary. Consequently, the electron temperature is constant at high altitudes owing to the dominance of thermal conduction.

For all the cases shown in Figure 12, thermoelectric heat transport corresponds to an upward flow of energy at all altitudes, but it can be a source or sink of heat depending on the shape of the electron density profile. For example, if we consider the solar minimum-winter case with $J_{\parallel} = -5 \times 10^{-5}$ amp m^{-2}, thermoelectric heat transport is a sink below 200 km, a source between 200 and 280 km, and a sink above 280 km. The effect of an increased magnitude of the return current is merely to enhance this result. Note that above 280 km for the $J_{\parallel} = -5 \times 10^{-5}$ amp m^{-2} curve, the electron temperature decreases with altitude up to 750 km with a gradient of about 1 K km^{-1} because of the cooling associated with thermoelectric heat transport. At 720 km, $T_e = 680$ K, which is lower than T_n (~ 750 K). Note also that T_e is much lower than T_i, which is 1500 K at 720 km. Above about 720 km, there is an abrupt change in the T_e gradient. This occurs because for the cases shown in Figure 12 we assumed that the total heat flux through the upper boundary was zero, and

therefore, a downward thermal conduction flux from the magnetosphere must balance the upward thermoelectric heat flux from the ionosphere at our upper boundary.

10. Future Direction

Significant progress has been made during the last decade in elucidating the basic physical and chemical processes governing ionospheric behavior. The bulk of the model studies, however, have been qualitative in nature, relying on emprical inputs, and they have concentrated on describing large-scale ionospheric features. Also, to date, only simple time-dependent electric field and particle precipitation patterns have been considered. In the near future our main emphasis will be on coupling ionospheric and thermospheric models so that coupling phenomena, time delays, and feedback mechanisms can be studied. We will also consider the more complicated time variations of the magnetospheric input parameters that are associated with geomagnetic storms and substorms, and we will begin a comprehensive study of small-scale ionospheric irregularities. In the more distant future, we will couple solar wind, magnetosphere, ionosphere and thermosphere models so that we can trace the flow of mass, momentum and energy from the sun to the earth's upper atmosphere. An integral part of these studies, of course, is a comparison of the model results with data obtained simultaneously from multiple observing sites so that the model results can be tested. Only in this way will we truly increase our understanding of the solar terrestrial system.

Acknowledgements

This research was supported by NASA grant NAGW-77 and by the University Research Initiative program under AFOSR contract F49620–86–C–0109 to Utah State University.

Appendix A

The conductivities in equation (61) have been derived by Conrad and Schunk (1979) for the case of arbitrarily large temperature differences between interacting species. These expressions are given by

$$K'_{st} = \frac{-F_{st} J_t}{H_{st}} \tag{A1}$$

$$K_{st} = \frac{C_{st} J_t}{H_{st}} \tag{A2}$$

$$R_{st} = \frac{C_{st} A_{ts} + F_{ts} A_{st}}{H_{st}} \tag{A3}$$

where

$$A_{st} = \frac{p_s \nu_{st} \mu_{st}}{m_t} \left\{ \frac{5}{2} \left[\frac{T_t}{T_{st}} + \frac{m_t}{m_s} \frac{T_{st}}{T_s} (1 - z_{st}) \right] + y_{st} \left(1 - \frac{T_t}{T_s} \right) - \frac{5}{2} \left(\frac{m_t}{\mu_{st}} \right) \right\} \tag{A4}$$

$$F_{st} = -\left\{ \frac{2 z''_{ss}}{5} \nu_{ss} + \nu_{st} \left[3 \left(\frac{\mu_{st}}{m_t} \right)^2 \left(\frac{T_t}{T_{st}} \right)^2 + B^{(3)}_{st} \left(z'_{st} - \frac{5}{2} z_{st} \right) - B^{(1)}_{st} \right.\right.$$
$$\left.\left. + \frac{\mu_{st}}{(m_s + m_t)} \frac{T_t}{T_{st}} \left[\frac{4}{5} z''_{st} - \frac{5}{2} \frac{T_s}{T_{st}} z_{st} \right] + \frac{5}{2} \frac{T_s}{T_{st}} \frac{\mu_{st}}{m_s} z_{st} \right] \right\} \tag{A5}$$

$$C_{st} = \nu_{st} \frac{\rho_s}{\rho_t} \left\{ 3 \left(\frac{\mu_{st}}{m_s} \right)^2 \left(\frac{T_s}{T_{st}} \right)^2 + B^{(3)}_{st} \left(z'_{st} - \frac{5}{2} z_{st} \right) + B^{(2)}_{st} - \frac{\mu_{st}}{m_s + m_t} \right.$$
$$\left. \cdot \frac{T_s}{T_{st}} \left[\frac{4}{5} \frac{m_t}{m_s} z''_{st} + \frac{5}{2} \frac{T_t}{T_{st}} z_{st} \right] + \frac{5}{2} \frac{T_s}{T_{st}} \frac{\mu_{st}}{m_s} z_{st} \right\} \tag{A6}$$

$$J_s = \frac{5}{2} \frac{k p_s}{m_s} \tag{A7}$$

$$H_{st} = F_{st} F_{ts} - C_{st} C_{ts} \tag{A8}$$

and where a simple interchange of indices will give the corresponding coefficient. For example, to get F_{ts}, just interchange t and s in equation (A5).

The additional expressions needed in equations (A1) to (A8) are given by

$$y_{st} = \frac{m_t}{m_s + m_t} \left[2 z''_{st} - 5 \frac{T_s}{T_{st}} - \frac{15}{2} \frac{m_s (1 - z_{st})}{m_s + m_t} \frac{(T_t - T_s)}{T_{st}} \right] \tag{A9}$$

$$B^{(1)}_{st} = \frac{m_t \mu_{st}}{(m_s + m_t)^2} \frac{T_t - T_s}{T_{st}} \left[\frac{4}{5} z'''_{st} - 2 z''_{st} + \frac{m_s}{m_t} \frac{T_t}{T_{st}} (6 - 11 z_{st}) \right] \tag{A10}$$

$$B^{(2)}_{st} = \frac{m_t \mu_{st}}{(m_s + m_t)^2} \frac{T_t - T_s}{T_{st}} \left[-\frac{4}{5} z'''_{st} + 2 z''_{st} + \frac{T_s}{T_{st}} (6 - 11 z_{st}) \right] \tag{A11}$$

$$B^{(3)}_{st} = \frac{m_t^2}{(m_s + m_t)^2} \left[1 + \frac{3 m_s^2}{(m_s + m_t)^2} \frac{(T_t - T_s)^2}{T_{st}^2} \right] \tag{A12}$$

$$T_{st} = \frac{m_t T_s + m_s T_t}{m_s + m_t} \tag{A13}$$

$$\mu_{st} = \frac{m_s m_t}{m_s + m_t} \tag{A14}$$

$$\rho_s = n_s m_s \tag{A15}$$

$$p_s = n_s k T_s. \tag{A16}$$

These expressions, in turn, depend on the ratio of certain collision integrals

$$z_{st} = 1 - \frac{2}{5}\frac{\Omega_{st}^{(1,2)}}{\Omega_{st}^{(1,1)}} \tag{A17}$$

$$z'_{st} = \frac{5}{2} + \frac{2}{5}\frac{\Omega_{st}^{(1,3)} - 5\Omega_{st}^{(1,2)}}{\Omega_{st}^{(1,1)}} \tag{A18}$$

$$z''_{st} = \frac{\Omega_{st}^{(2,2)}}{\Omega_{st}^{(1,1)}} \tag{A19}$$

$$z'''_{st} = \frac{\Omega_{st}^{(2,3)}}{\Omega_{st}^{(1,1)}} \tag{A20}$$

where

$$\Omega_{in}^{(1,1)} = \left(\frac{kT_{in}}{2\pi\mu_{in}}\right)^{1/2}\left[39.84B^2 - 17.85AB + 2A^2 + (8.923B^2 - 2AB)\cdot\log_{10}\frac{T_{in}}{M} + \frac{B^2}{2}\left(\log_{10}\frac{T_{in}}{M}\right)^2\right] \tag{A21}$$

$$\Omega_{in}^{(1,2)} = 3\left(\frac{kT_{in}}{2\pi\mu_{in}}\right)^{1/2}\left[41.14B^2 - 18.13AB + 2A^2 + (9.067B^2 - 2AB)\cdot\log_{10}\frac{T_{in}}{M} + \frac{B^2}{2}\left(\log_{10}\frac{T_{in}}{M}\right)^2\right] \tag{A22}$$

$$\Omega_{in}^{(1,3)} = 12\left(\frac{kT_{in}}{2\pi\mu_{in}}\right)^{1/2}\left[42.12B^2 - 18.35AB + 2A^2 + (9.176B^2 - 2AB)\cdot\log_{10}\frac{T_{in}}{M} + \frac{B^2}{2}\left(\log_{10}\frac{T_{in}}{M}\right)^2\right] \tag{A23}$$

$$\Omega_{in}^{(2,2)} = 0.8\pi\left(\frac{\eta e^2}{\mu_{in}}\right)^{1/2} \tag{A24}$$

$$\Omega_{in}^{(2,3)} = 3.5\Omega_{in}^{(2,2)} \tag{A25}$$

and where $A = 1.1 \times 10^{-7}$ cm and $B = 0.95 \times 10^{-8}$ cm, η is the neutral atom polarizability—this is 0.77×10^{-24} cm^3 for atomic oxygen—and M is the atomic weight for oxygen (16.0) and the other variables are the same as defined elsewhere in the paper.

For neutral-neutral interactions, only two values are actually needed in the computations,

$$\nu_{nn} = \frac{8n_n}{3\sqrt{\pi}}\left(\frac{kT_n}{m_n}\right)^{\frac{1}{2}}(\pi\sigma^2) \tag{A26}$$

$$z''_{nn} = 2 \tag{A27}$$

where $\pi\sigma^2$ is the hard sphere cross-section. This model deals with atomic oxygen–atomic oxygen interactions, and the following value was used:

$$\pi\sigma^2 = 1.87 \times 10^5 \frac{\sqrt{k\pi m_n}}{2T_n^{0.21}} \tag{A28}$$

where m_n is the mass of atomic oxygen and T_n is the neutral temperature.

References

Albritton, D. L., Dotan, I., Lindinger, W., McFarland, M., Tellinghuiser, J. and Fehsenfeld, F. C. (1977), *Effects of ion speed distributions in flow drift tube studies on ion-neutral reactions.* J. Chem. Phys. *66*, 410.

Anderson, D. N. (1981), *Modeling the ambient, low latitude F region ionosphere—a review.* J. Atmos. Terr. Phys. *43*, 753–762.

Bailey, G. J., Moffett, R. J. and Murphy, J. A. (1978), *Interhemispheric flow of thermal plasma in a closed magnetic flux tube at mid-latitudes under sunspot minimum conditions.* Planet. Space Sci. *26*, 753–765.

Banks, P. M. and Kockarts, G. (1973), *Aeronomy* (Academic, New York).

Chandler, M. O., Behnke, R. A., Nagy, A. F., Fontheim, E. G., Richards, P. G. and Torr, D. G. (1983), *Comparison of measured and calculated low-latitude ionospheric properties.* J. Geophys. Res. *88*, 9187–9196.

Chapman, S. (1931), *The absorption and dissociative or ionizing effect of monochromatic radiation in an atmosphere on a rotating Earth-II grazing incidence.* Proc. Phys. Soc. (London) *43*, 483–501.

Chapman, S. and Cowling, T. G. (1970), *The mathematical theory of non-uniform gases* (Cambridge University Press, Cambridge).

Chen, W. M. and Harris, R. D. (1971), *An ionospheric E-region night-time model.* J. Atmos. Terr. Phys. *33*, 1193–1207.

Comes, F. J. and Elzer, A. (1968), *Photoionisationsuntersuchungen an Atomstrahlen, III, der Ionisierungsquerschnitt des Atomaness Stickstoff.* Z. Nutr. *23*, 133.

Conrad, J. R. and Schunk, R. W. (1979), *Diffusion and heat flow equations with allowance for large temperature differences between interacting species.* J. Geophys. Res. *84*, 811–822.

Crank, J. and Nicolson, P. (1947), *A practical method for numerical evaluation of solutions of partial differential equations of the heat-conduction type.* Cambridge Philos. Soc. *43*, 50–67.

Dalgarno, A. (1968), *Collisions in the ionosphere.* Advan. At. Mol. Phys. *4*, 381–410.

Fehsenfeld, F. C. (1977), *The reactions of O_2^+ with atomic nitrogen and NO^+ H_2O and NO_2^+ with atomic oxygen.* Planet. Space Sci. *25*, 195.

FEHSENFELD, F. C., DUNKIN, D. B. and FERGUSON, E. E. (1970), *Rate constants for the reaction of CO_2^+ with O, O_2 and NO; N_2^+ with O and NO; and O_2^+ with NO.* Planet. Space Sci. *18*, 1267–1269.

FELDSTEIN, Y. I. and STARKOV, G. V. (1967), *Dynamics of auroral belt and polar geomagnetic disturbances.* Planet. Space Sci. *15*, 209–229.

FITE, W. L. (1969), *Positive ion reactions.* Can. J. Chem. *47*, 1797–1807.

FOSTER, J. C. (1983), *An empirical electric field model derived from chatanika radar data.* J. Geophys. Res. *88*, 981–987.

HEDIN A. E. *et al.* (1977*a*), *A global thermospheric model based on mass spectrometer and incoherent scatter data, MSIS 1, N_2 density and temperature.* J. Geophys. Res. *82*, 2139–2147.

HEDIN, A. E. *et al.* (1977*b*), *A global thermospheric model based on mass spectrometer and incoherent scatter data, MSIS 2, composition.* J. Geophys. Res. *82*, 2148–2156.

HEELIS, R. A., LOWELL, J. K. and SPIRO, R. W. (1982), *A model of the high-latitude ionospheric convection pattern.* J. Geophys. Res. *87*, 6339–6345.

HENRY, R. J. W. (1968), *Photoionization cross sections for N and O^+.* J. Chem. Phys. *48*, 3635.

HENRY, R. J. W., BURKE, P. G. and SINFAILAM, A. L. (1969), *Scattering of electrons by C, N, O, N^+, O^+ and O^{++}.* Phys. Rev. *178*, 218.

HEPPNER, J. P. (1977), *Empirical models of the high-latitude electric fields.* J. Geophys. Res. *82*, 1115–1125.

HEROUX, L. and HINTEREGGER, H. E. (1978), *Aeronomical reference spectrum for solar UV below 2000 A.* J. Geophys. Res. *83*, 5305–5308.

HINTEREGGER, H. E., BEDO, D. E., MANSON, J. E. and SKILLMAN, D. R. (1977), *EUV flux variations with solar rotation observed during 1974–1976 from the AE-C satellite.* Space Res. *17*, 533–544.

HOEGY, W. R. (1976), *New fine structure cooling rate.* Geophys. Res. Lett. *3*, 541–544.

HUNTRESS, W. T. and ANICICH, V. G. (1976), *On the reaction of N^+ ions with O_2,* Geophys. Res. Lett *3*, 317.

KAMIDE, Y., CRAVEN, J. D., FRANK, L. A., AHN, B.-H. and AKASOFU, S.-I. (1986), *Modeling substorm current systems using conductivity distributions inferred from DE auroral images.* J. Geophys. Res. *91*, 11235–11256.

KIRBY-DOCKEN, K., CONSTANTINIDES, E. R., BABEU, S., OPPENHEIMER, M. and VICTOR, G. A. (1978), *Photoionization and photoabsorption cross sections of thermospheric species: He, O, N_2 and O_2.* Atomic Data and Nuclear Data Tables.

KNUDSEN, W. C., BANKS, P. M., WINNINGHAM, J. D. and KLUMPAR, D. M. (1977), *Numerical model of the convecting F_2 ionosphere at high latitudes.* J. Geophys. Res. *82*, 4784–4792.

KOSMIDER, R. G. and HASTED, J. B. (1975), *Collision processes of drifting O^+ and N^+ ions.* J. Phys. B. *8*, 273.

LINDINGER, W., FEHSENFELD, F. C., SCHMELTEKOPF, A. L. and FERGUSON, E. E. (1974), *Temperature dependence of some ionospheric ion-neutral reactions from 300°–900° K.* J. Geophys. Res. *79*, 4753.

MATSUSHITA, S. and XU, W.-Y. (1982), *Equivalent ionospheric current systems representing IMF sector effects on the polar geomagnetic field.* Planet. Space Sci. *30*, 641–656.

MCELROY, M. B. (1967), *Atomic nitrogen ions in the upper atmosphere.* Planet. Space Sci. *15*, 457.

MCFARLAND, M., ALBRITTON, D. L., FEHSENFELD, F. C., FERGUSON, E. E. and SCHMELTEKOPF, A. L. (1973), *Flow-drift technique for ion mobility and ion-molecule reaction rate constant measurements. II, positive ion reactions of N^+, O^+, and N_2^+ with O_2 and O^+ with N_2 + O reaction.* J. Chem. Phys. *59*, 6620–6628.

MCFARLAND, M., ALBRITTON, D. L., FEHSENFELD, F. C., FERGUSON, E. E. and SCHMELTEKOPF, A. L. (1974), *Energy dependence and branching ratio of the N_2^+ + O reaction.* J. Geophys. Res. *79*, 2925.

MEHR, F. J. and BIONDI, M. A. (1969), *Electron temperature dependence of recombination of O_2^+ and N_2^+ ions with electrons.* Phys. Rev. *181*, 264.

MOFFETT *et al.* (1986), Adv. Space Res. *6*, 153.

MURPHY, J. A., BAILEY, G. L. and MOFFETT, R. J. (1976), *Calculated daily variations of O^+ and H^+ at Mid-latitudes.* J. Atmos. Terr. Phys. *38*, 351–364.

PRASAD, S. S. and FURMAN, D. R. (1973), *Electron cooling by molecular oxygen.* J. Geophys. Res. *78*, 6701–6707.

QUEGAN, S. BAILEY, G. J., MOFFETT, R. J., HEELIS, R. A., FULLER-ROWELL, T. J., REES, D. and SPIRO, R. W. (1982), *A theoretical study of the distribution of ionization in the high-latitude ionosphere and the plasmasphere: first results on the mid-latitude trough and the light-ion trough.* J. Atmos. Terr. Phys. *44*, 619–640.

RAITT, W. J., SCHUNK, R. W. and BANKS, P. M. (1978*a*), *Helium ion outflow from the terrestrial ionosphere.* Planet. Space Sci. *26*, 255–268.

RAITT, W. J., SCHUNK, R. W. and BANKS, P. M. (1978*b*), *Quantitative calculations of helium ion escape fluxes from the polar ionospheres.* J. Geophys. Res. *83*, 5617–5623.

REES, M. H., JONES, R. A. and WALKER, J. C. G. (1971), *The influence of field-aligned currents on auroral electron temperatures.* Planet. Space Sci. *19*, 313–325.

RICHARDS P. G. and TORR, D. G. (1984), *An investigation of the consistency of the ionospheric measurements of the photoelectron flux and solar EUV flux.* J. Geophys. Res. *89*, 5625–5635.

RISHBETH, H. and GARRIOTT, O. K. (1969), *Introduction to Ionospheric Physics* (Academic Press, New York).

RISHBETH, H. and HANSON, W. B. (1974), *A comment on plasma pile-up in the F-region.* J. Atmos. Terr. Phys. *36*, 703–706.

ROBLE, R. G. (1975), *The calculated and observed diurnal variation of the ionosphere over Millstone Hill on March 23–24, 1970.* Planet. Space Sci. *23*, 1017–1030.

ROBLE, R. G. and REES, M. H. (1977), *Time-dependent studies of the aurora: effects of particle precipitation on the dynamic morphology of ionospheric and atmospheric properties.* Planet. Space Sci. *25*, 991–1010.

RUTHERFORD J. A. and VROOM, D. A. (1971), *Effect of metastable $O^+(^2D)$ on reactions of O^+ with nitrogen molecules.* J. Chem. Phys. *55*, 5622.

SCHUNK, R. W. (1975), *Transport equations for aeronomy.* Planet. Space Sci. *23*, 437–485.

SCHUNK, R. W. (1977), *Mathematical structure of transport equations for multispecies flows.* Rev. Geophys. Space Phys. *15*, 429–445.

SCHUNK, R. W. (1983), *Solar-terrestrial physics* (D. Reidel, Dordrecht), pp. 609–676.

SCHUNK, R. W. (1987), *Interactions between the polar ionosphere and thermosphere.* Physica Scripta, *T18*, 256–275.

SCHUNK, R. W. and NAGY, A. F. (1978), *Electron temperatures in the F-region of the ionosphere: theory and observations.* Rev. Geophys. Space Phys. *16*, 355–399.

SCHUNK, R. W. and RAITT, W. J. (1980), *Atomic nitrogen and oxygen ions in the daytime high-latitude F-region.* J. Geophys. Res. *85*, 1255–1272.

SCHUNK R. W. and SOJKA, J. J. (1982), *Ion temperature variations in the daytime high-latitude F-region.* J. Geophys. Res. *87*, 5169–5183.

SCHUNK, R. W. and SOJKA, J. J. (1987), *Ionospheric features induced by magnetospheric processes*, In: *Quantitative modeling of magnetosphere-ionosphere coupling processes.* Kyoto, Japan, 11–16.

SCHUNK, R. W. and WALKER, J. C. G. (1970), *Transport properties of the ionospheric electron gas.* Planet. Space Sci. *18*, 1535–1550.

SCHUNK, R. W. and WALKER, J. C. G. (1973), *Theoretical ion densities in the lower ionosphere.* Planet. Space Sci. *21*, 1875–1896.

SCHUNK, R. W., RAITT, W. J. and BANKS, P. M. (1975), *Effect of electric fields on the daytime high-latitude E- and F-regions.* J. Geophys. Res. *80*, 3121–3130.

SCHUNK, R. W., BANKS, P. M. and RAITT, W. J. (1976), *Effects of electric fields and other processes upon the nighttime high latitude F-layer.* J. Geophys. Res. *81*, 3271–3282.

SCHUNK, R. W., SOJKA, J. J. and BOWLINE, M. D. (1986), *Theoretical study of the electron temperature in the high latitude ionosphere for solar maximum and winter conditions.* J. Geophys. Res. *91*, 12041–12054.

SCHUNK, R. W., SOJKA, J. J. and BOWLINE, M. D. (1987), *Theoretical study of the effect of ionospheric return currents on the electron temperature.* J. Geophys. Res. *92*, 6013–6022.

SMITH, F. L. and SMITH, C. (1972), *Numerical evaluation of Chapman's grazing incidence integral* ch(X,χ). J. Geophys. Res. *77*, 3592–3597.

SOJKA, J. J. and SCHUNK, R. W. (1985), *A theoretical study of the global F region for June solstice, solar maximum, and low magnetic activity.* J. Geophys. Res. *90*, 5285–5298.

SOJKA, J. J. and SCHUNK, R. W. (1987), *Magnetospheric control of the bulk ionospheric plasma*, in: Proceedings of the AGARD/NATO Symposium on 'The aerospace environment at high altitudes and its implications for spacecraft charging and communications', Hague, The Netherlands, 2.1–2.13.

SOJKA, J. J., RAITT, W. J. and SCHUNK, R. W. (1981*a*), *A theoretical study of the high-latitude winter F-region at solar minimum for low magnetic activity.* J. Geophys. Res. *86*, 609–621.

SOJKA, J. J., RAITT, W. J. and SCHUNK, R. W. (1981*b*), *Theoretical predictions for ion composition in the high-latitude winter F-region for solar minimum and low magnetic activity.* J. Geophys. Res. *86*, 2206–2216.

SOJKA, J. J., RASMUSSEN, C. E. and SCHUNK, R. W. (1986), *An interplanetary magnetic field dependent model of the ionospheric convection electric field.* J. Geophys. Res. *91*, 11281–11290.

SPIRO, R. W., REIFF, P. H. and MAHER, L. H. (1982), *Precipitating electron energy flux and auroral zone conductances: An empirical model.* J Geophys. Res *87*, 8215–8227.

STERLING, D. L., HANSON, W. B., MOFFETT, R. J. and BAXTER, R. G. (1969), *Influence of electromagnetic drifts and neutral air winds on some features of the F_2 region.* Radio Sci. *4*, 1005–1023.

ST.-MAURICE J.-P. and TORR, D. G. (1978), *Nonthermal rate coefficients in the ionosphere: the reactions of O^+ with N_2, O_2, and NO.* J. Geophys. Res. *83*, 969.

STROBEL, D. F. and MCELROY, M. B. (1970), *The F_2-layer at middle latitudes.* Planet. Space Sci. *18*, 1181–1202.

STUBBE, P. and VARNUM, W. S. (1972), *Electron energy transfer rates in the ionosphere.* Planet. Space Sci. *20*, 1121–1126.

TORR, D. G. and ORSINI N. (1978), *The effect of N_2^+ recombination on the aeronomic determination of the charge exchange rate coefficient of $O^+(^2D)$ with N_2.* Geophys. Res. Lett. *5*, 657.

TORR, D. G., TORR, M. R., WALKER, J. C. G., BRACE, L. H., BRINTON, H. C., HANSON, W. B, HOFFMANN, R. H., NIER, A. O. and OPPENHEIMER, M. (1976*a*), *Recombination of NO^+ in the ionosphere.* Geophys. Res. Lett. *3*, 209.

TORR, D. G., TORR, M. R., WALKER, J. C. G., NIER, A. O., BRACE, L. H. and BRINTON, H. C. (1976*b*), *Recombination of O_2^+ in the ionosphere.* J. Geophys. Res. *81*, 5578.

TORR, D. G., ORSINI, N. TORR, M. R., HANSON, W. B., HOFFMANN, J. H. and WALKER, J. C. G. (1977), *Determination of the rate coefficient for the $N_2^+ + O$ reaction in the ionosphere.* J. Geophys. Res. *82*, 1631.

TORR, M. R., TORR, D. G., ONG, R. A. and HINTEREGGER, H. E. (1979*a*), *Ionization frequencies for major thermospheric constituents as a function of solar cycle 21.* Geophys. Res. Lett. *10*, 771–774.

TORR, D. G., TORR, M. R., BRINTON, H. C., BRACE, L. H., SPENCER, N. W., HEDIN, A. E., HANSON, W. B., HOFFMANN, J. H., NIER, A. O., WALKER, J. C. G. and RUSCH, D. W. (1979*b*), *An experimental and theoretical study of the mean diurnal variation of O^+, NO^+, O_2^+, and N_2^+ ions in the mid-latitude F_1 layer of the ionosphere.* J. Geophys. Res. *84*, 3360–3372.

VOLLAND, H. (1978), *A model of the magnetospheric electric convection field.* J. Geophys. Res. *83*, 2695–2699.

WALLIS, D. D. and BUDZINSKI, E. E. (1981), *Empirical models of height integrated conductivities.* J. Geophys. Res. *86*, 125–137.

WALLS, F. L. and DUNN, G. H. (1974), *Measurement of total cross sections for electron recombination with NO^+ and O_2^+ using ion storage techniques.* J. Geophys. Res. *79*, 1911–1915.

WATKINS, B. J. (1978), *A numerical computer investigation of the polar F region ionosphere.* Planet. Space Sci. *26*, 559–569.

(Received 11th May 1987, revised/accepted 8th September 1987)